Theory of the evolution of phonon spectra and elastic constants from graphene to graphite

K. H. Michel[1] and B. Verberck[1,2]
[1]*Departement Fysica, Universiteit Antwerpen, Groenenborgerlaan 171, 2020 Antwerpen, Belgium*
[2]*Institut für Festkörperforschung, Forschungszentrum Jülich, 52425 Jülich, Germany*
(Received 25 April 2008; revised manuscript received 11 July 2008; published 20 August 2008)

We present a unified theory of the phonon dispersions and elastic properties of graphene, graphite, and graphene multilayer systems. Starting from a fifth-nearest-neighbor force-constant model derived from full in-plane phonon dispersions of graphite [Mohr *et al.*, Phys. Rev. B **76**, 035439 (2007)], we use Born's long-wave method to calculate the tension and bending coefficients of graphene. Extending the model by interplanar interactions, we study the phonon dispersions and the elastic constants of graphite, and the phonon spectra of graphene multilayers. We find that the inner displacement terms due to sublattice shifts between inequivalent C atoms are quantitatively important in determining the elastomechanical properties of graphene and of graphite. The overall agreement between theory and experiment is very satisfactory. We investigate the evolution from graphene to graphite by studying the increase in the $\omega_{B_{2g_1}}^{(N)}$ rigid plane optical mode as a function of the number of layers N. At $N=10$ the graphite value $\omega_{B_{2g_1}} \approx 127$ cm^{-1} is attained within a few percent.

DOI: 10.1103/PhysRevB.78.085424 PACS number(s): 62.20.−x

I. INTRODUCTION

Graphite, the stable form of solid carbon under ambient conditions, has a broad range of applications in industry. It is also the basic material for the synthesis of different nanoscopic materials such as fullerenes and carbon nanotubes.[1,2] The physical properties and the chemical flexibility are a direct consequence of the layer structure of graphite. Carbon atoms within a plane are strongly bonded by sp^2 hybridizations and form a hexagonal (honeycomb) network called graphene. The three-dimensional (3D) graphite is obtained by a stacking of the two-dimensional (2D) graphene layers in an $\ldots\alpha\beta\alpha\beta\ldots$ sequence. The interaction between layers is ascribed to weak van der Waals forces. Due to the large difference between intralayer and interlayer forces between C atoms, the physical properties of graphite are very anisotropic. A direct signature of this anisotropy is manifest in the lattice dynamics measured by inelastic neutron scattering (INS) (Refs. 3 and 4): vibrational modes that correspond to relative atomic displacements in the same basal plane have high frequencies whereas modes in which the basal planes move as rigid units have low frequencies. In addition to the early INS work, we mention related experimental work on elastic constants and optical phonons,[5–7] and theoretical work on lattice dynamics.[8–11] A comprehensive review on the physics of graphite until 1981 is found in the book by Kelly.[12] In the last decades advances have been made due to the use of experimental methods[13] and of progress in first-principles calculations.[14,15]

Due to the crystallographic structure of graphite, a 2D model of the lattice, i.e., graphene, as used in early work,[16–18] has proven to be an adequate approximation for the explanation of electrical and magnetic properties.[19] More recently the electronic band structure and the lattice dynamics of graphene have been used as basis concepts for the understanding of the electronic and vibrational properties of single-wall carbon nanotubes.[2,20,21] Indeed a single-wall nanotube is obtained by rolling up a graphene sheet into a hollow cylinder. Hence graphene has been an extremely useful theoretical paradigm. On the other hand the isolation of a single graphene sheet as materialization of a 2D crystal had eluded experiment, in agreement with a fundamental theorem about the absence of crystalline order in two dimensions.[22] The experimental discovery of graphene and other free-standing 2D atomic crystals[23,24] came as a great surprise; since then 2D crystals have become a topic of intense experimental and theoretical research in condensed-matter physics and materials science.

While in the years following the discovery of graphene, the unusual electronic properties of graphene were at the center of interest;[25] the thermoelastic and lattice-dynamical properties are getting increasing attention. These studies are essential for the understanding of the stability of graphene as a truly 2D crystal.[26,27]

The purpose of the present paper is to give a unified theoretical description of the lattice dynamics, and the elastic stretching and bending of graphene, of the phonons and elastic constants of graphite, and of the phonons of multilayer graphene systems. Our theoretical study is complementary to recent experimental inelastic x-ray scattering (IXS) work on the elasticity[28] and the full in-plane phonon dispersion of graphite.[29,30]

II. ELEMENTS OF LATTICE DYNAMICS

We recall some basic concepts of lattice dynamics of a nonprimitive non-ionic 3D crystal.[31,32] Later on we will consider the cases of 2D and multilayer crystals.

The crystal consists of N unit cells with each cell containing s atoms. The positions of the unit cells are fixed by the lattice vectors,

$$\vec{X}(\vec{n}) = n_1\vec{a}_1 + n_2\vec{a}_2 + n_3\vec{a}_3. \quad (1)$$

Here $\vec{a}_l$, with $l=1,2,3$, are three noncoplanar basis vectors while the triplet of integers $\vec{n}=(n_1,n_2,n_3)$ labels the unit

cells. The equilibrium positions of the atoms are given by

$$\vec{X}(\vec{n}\kappa) = \vec{X}(\vec{n}) + \vec{r}^{\kappa}. \tag{2}$$

Here $\vec{r}^{\kappa}$, where $\kappa = 1, 2, \ldots, s$, specifies the location of the κth atom in the unit cells. We write $u_i(\vec{n}\kappa)$ for the ith Cartesian component ($i=x,y,z$) of the instantaneous displacement vector of the atom $(\vec{n}\kappa)$ away from its equilibrium position.

The crystal potential energy Φ is a function of the instantaneous positions $\vec{R}(\vec{n}\kappa)=\vec{X}(\vec{n}\kappa)+\vec{u}(\vec{n}\kappa)$ of the atoms. The harmonic part of the potential then reads

$$V^{(2)} = \frac{1}{2}\sum_{\vec{n}\kappa}\sum_{\vec{n}'\kappa'}\sum_{ij}\Phi_{ij}(\vec{n}\kappa;\vec{n}'\kappa')u_i(\vec{n}\kappa)u_j(\vec{n}'\kappa'). \tag{3}$$

The coupling parameters $\Phi_{ij}(\vec{n}\kappa;\vec{n}'\kappa')$ are the second derivatives of the potential energy with respect to the displacements, taken at the equilibrium positions.

The kinetic energy of the crystal is given by

$$T = \sum_{\vec{n},\kappa}\sum_{i}\frac{p_i(\vec{n}\kappa)^2}{M_\kappa}, \tag{4}$$

where $p_i(\vec{n}\kappa)$ are the components of the atomic momentum conjugate to $u_i(\vec{n},\kappa)$ and where M_κ is the mass of the κth atom. The displacements are function of time; the crystal dynamics is described by a system of $3sN$ coupled equations of motion

$$M_\kappa \ddot{u}_i(\vec{n}\kappa) = -\sum_{\vec{n}'\kappa' j}\Phi_{ij}(\vec{n}\kappa;\vec{n}'\kappa')u_j(\vec{n}'\kappa'). \tag{5}$$

Under the assumption that the crystal is extended in all three directions: $\vec{a}_1$, $\vec{a}_2$, and $\vec{a}_3$, the Born-von Karman periodic boundary conditions apply and one introduces Fourier transforms in space. In addition one chooses a periodic time dependence with frequency ω and writes

$$u_i(\vec{n}\kappa) = \frac{1}{\sqrt{M_\kappa N}}\sum_{\vec{q}}u_i^{\kappa}(\vec{q})e^{i\vec{q}\cdot\vec{X}(\vec{n}\kappa)-i\omega t}. \tag{6}$$

Here $\vec{q}$ is a wave vector in the 3D Brillouin zone. The equation of motion reads

$$\omega^2 u_i^{\kappa}(\vec{q}) = \sum_{\kappa' j}D_{ij}^{\kappa\kappa'}(\vec{q})u_j^{\kappa'}(\vec{q}), \tag{7}$$

where $D_{ij}^{\kappa\kappa'}$ are the elements of the dynamical matrix $D(\vec{q})$:

$$D_{ij}^{\kappa\kappa'}(\vec{q}) = \frac{1}{\sqrt{M_\kappa M_{\kappa'}}}\sum_{\vec{n}'}\Phi_{ij}(\vec{n}\kappa;\vec{n}'\kappa')e^{i\vec{q}\cdot[\vec{X}(\vec{n}'\kappa')-\vec{X}(\vec{n}\kappa)]}. \tag{8}$$

The $3s\times 3s$ dynamical matrix is Hermitian. The eigenvalues (optical and acoustic phonon branches) are obtained by solving the secular equation

$$|1\omega^2 - D(\vec{q})| = 0. \tag{9}$$

Knowledge of the dynamical matrix $D(\vec{q})$ allows one to derive expressions of the macroscopic elastic constants in terms of the interatomic coupling parameters by using Born's long-wave method.[32] One starts from the series expansion in powers of small $\vec{q}$:

$$D_{ij}^{\kappa\kappa'}(\vec{q}) = D_{ij}^{\kappa\kappa'(0)} + i\sum_k D_{ij,k}^{\kappa\kappa'(1)}q_k + \frac{1}{2}\sum_{kl}D_{ij,kl}^{\kappa\kappa'(2)}q_k q_l + \ldots. \tag{10}$$

In the long-wavelength limit, the acoustic dynamical matrix has elements

$$\hat{D}_{ij}(\vec{q}) = \frac{1}{\rho}\sum_{kl}[(ij,kl)+(ik,jl)]q_k q_l. \tag{11}$$

Here $\rho=\frac{1}{v_c}\Sigma_\kappa M_\kappa$ is the mass density of the crystal with v_c as the volume of the primitive unit cell. The quantities $[ij,kl]$ and (ik,jl) are given by

$$[ij,kl] = \frac{1}{2v_c}\sum_{\kappa\kappa'}(M_\kappa M_\kappa)^{1/2}D_{ij,kl}^{\kappa\kappa'(2)}, \tag{12}$$

and

$$(ik,jl) = -\frac{1}{v_c}\sum_{\kappa\kappa'}\sum_{hp}\Gamma_{hp}^{\kappa\kappa'}\left[\sum_{\kappa''}(M_{\kappa''})^{1/2}D_{hi,k}^{\kappa\kappa''(1)}\right]\times\left[\sum_{\kappa'''}(M_{\kappa'''})^{1/2}D_{pj,l}^{\kappa'\kappa'''(1)}\right], \tag{13}$$

with

$$\Gamma_{hp}^{\kappa\kappa'} = \sum_{\lambda}\frac{w^{(\lambda)}(\kappa h)w^{(\lambda)}(\kappa' p)}{\omega_\lambda^2}, \tag{14}$$

where ω_λ and $w^{(\lambda)}$ being the optical eigenfrequencies and eigenvectors of the singular matrix $D(\vec{q}=\vec{0})$. The quantities (ij,kl) account for the elastic energy due to relative shifts between different sublattices; they are also referred to as inner displacement terms. These internal strain contributions, which are necessary to compensate the external forces in the interior of the system,[33] are different from zero if the atomic equilibrium positions are not centers of symmetry, as is the case for graphite and graphene. In Secs. IV and V we will see that the inner displacements are quantitatively important in determining the numerical values of the tension coefficients of graphene and for the elastic constants of graphite. Provided that the Huang conditions are satisfied, the elastic constants are given by[32]

$$C_{ij,kl} = [ik,jl] + [jk,il] - [ij,kl] + (ij,kl). \tag{15}$$

In principle, the knowledge of the crystal potential Φ allows the calculation of the dynamical matrix. A particular simple case is the central-force potential where Φ is a sum of two-atom potentials that depend only on the separation between the atoms. The harmonic potential then reads

$$V^{(2)} = \frac{1}{4}\sum_{\vec{n}\kappa}\sum_{\vec{n}'\kappa'}{}'\sum_{ij}\phi_{ij}(\vec{n}\kappa;\vec{n}'\kappa')u_i(\vec{n}\kappa;\vec{n}'\kappa')u_j(\vec{n}\kappa;\vec{n}'\kappa'), \tag{16}$$

with $\vec{u}(\vec{n}\kappa;\vec{n}'\kappa')=\vec{u}(\vec{n}\kappa)-\vec{u}(\vec{n}'\kappa')$. The prime at the summation sign excludes $(\vec{n}\kappa)=(\vec{n}'\kappa')$. The atomic force constants $\phi_{ij}(\vec{n}\kappa;\vec{n}'\kappa')$ are the second derivatives of the pair potential with respect to the atomic separations, taken at the equilib-

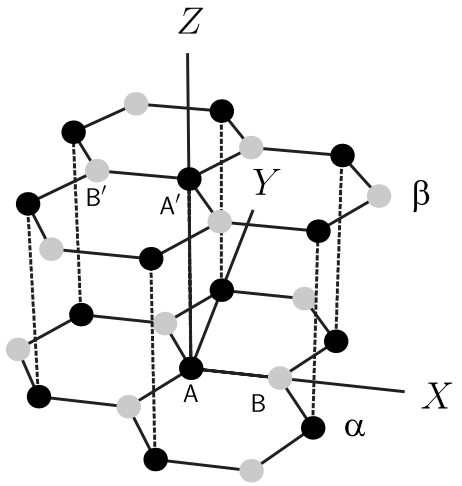

FIG. 1. Two neighboring layers, α and β, of graphite.

rium positions. The force constants $\phi_{ij}(\vec{n}\kappa;\vec{n}'\kappa')$ are related to the coupling parameters $\Phi_{ij}(\vec{n}\kappa;\vec{n}'\kappa')$ by

$$\Phi_{ij}(\vec{n}\kappa;\vec{n}\kappa) = \sum_{\vec{n}'\kappa}{}' \phi_{ij}(\vec{n}\kappa;\vec{n}'\kappa'), \tag{17a}$$

$$\Phi_{ij}(\vec{n}\kappa;\vec{n}'\kappa') = -\phi_{ij}(\vec{n}\kappa;\vec{n}'\kappa'), (\vec{n}\kappa) \neq (\vec{n}'\kappa'). \tag{17b}$$

In practice the situation is more complicated as a consequence of the covalent interatomic interactions within graphene layers. Hence the lattice dynamics of graphite is often described in terms of force constants, which are determined from the experimental phonon spectrum.[4,8,9,11] On the other hand some macroscopic properties such as the cohesive energy of graphite are related to the interplane van der Waals forces and have been treated in terms of Lennard-Jones (LJ) potentials.[34] In the following we will use force-constant parameters for the intraplane[30] and for the nearest-neighbor out-of-plane atom-atom interactions; further-neighbor out-of-plane interactions are described by a LJ potential.[35]

III. PHONONS IN GRAPHENE AND GRAPHITE

We now study the particular cases of graphite (3D) and graphene (2D). We recall that the graphite crystal has a 180° screw axis perpendicular to the graphene basal planes. We use a Cartesian system of axes (X,Y,Z) such that the screw axis is along the Z direction and perpendicular to the (X,Y) basal planes. Each graphene plane has a 2D hexagonal crystal structure and contains two inequivalent C atoms, called A and B, per unit cell (see Fig. 1). We label the graphene unit cells by a pair of indices $(n_1,n_2)=\vec{n}_\perp$ while $\vec{a}_1$ and $\vec{a}_2$ are in-plane basis lattice vectors with length $a=\sqrt{3}a_{CC}$, where $a_{CC}=1.42$ Å is the length of a C-C bond. The equilibrium position of the κth atom in the $\vec{n}_\perp$th unit cell then reads

$$\vec{X}(\vec{n}_\perp\kappa) = \vec{X}(\vec{n}_\perp) + \vec{r}^{\kappa}, \quad \kappa = A,B. \tag{18}$$

Here $\vec{r}^{A}=(0,0)$ and $\vec{r}^{B}=(a/\sqrt{3},0)$ in Cartesian coordinates while $\vec{X}(\vec{n}_\perp)=n_1\vec{a}_1+n_2\vec{a}_2$.

Similar graphene layers in graphite are stacked with corresponding A and B atoms above each other with a distance $c=6.70$ Å apart along the Z direction. We call these layers, labeled by an index $n_z=1,2,\ldots,N_z$, the α planes. Halfway between these layers are graphene sheets called βplanes. Because of the 180° rotation, the B' atoms in the β planes do not lie in line with the B atoms. We label the unit cells of graphite by indices $\vec{n}=(\vec{n}_\perp,n_z)\equiv(n_1,n_2,n_z)$ with corresponding lattice vectors

$$\vec{X}(\vec{n}_\perp,n_z) = n_1\vec{a}_1 + n_2\vec{a}_2 + n_z\vec{c}. \tag{19}$$

Each unit cell contains four atoms. The equilibrium position of the κth atom in the cell is given by

$$\vec{X}(\vec{n}_\perp,n_z,\kappa) = \vec{X}(\vec{n}_\perp,n_z) + \vec{r}^{\kappa}, \tag{20}$$

where $\vec{r}^{A}=(0,0,0)$, $\vec{r}^{B}=(a/\sqrt{3},0,0)$, $\vec{r}^{A'}=(0,0,c/2)$, and $\vec{r}^{B'}=(-a/\sqrt{3},0,c/2)$, for $\kappa=$ A, B, A', or B', respectively (Fig. 1). Since in the following we will only consider C atoms with average mass $M=12.02\times1.66\times10^{-24}$ g, we will drop the index κ on the mass.

The 3D Brillouin zone of graphite is shown in Fig. 2. The 2D Brillouin zone of graphene corresponds to the plane through the points Γ, K, and M.

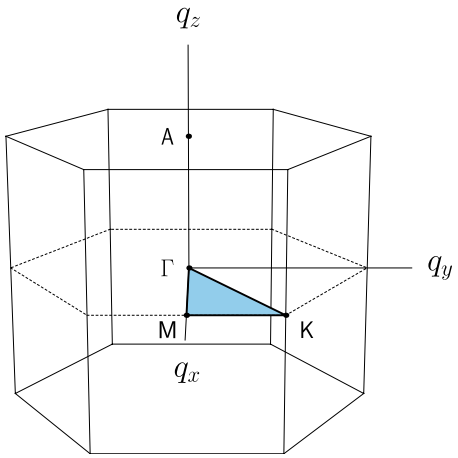

FIG. 2. (Color online) Brillouin zone of graphite.

A. Graphene

The formalism of the last section is readily applied to the case of graphene. We assume that the 2D crystal is sufficiently extended such that periodic boundary conditions apply in two directions. We denote the force constants by $f_{ij}(\vec{n}_\perp\kappa;\vec{n}'_\perp\kappa')$ and write $F(\vec{q}_\perp)$ for the 6×6 dynamical matrix where $\vec{q}_\perp$ is a vector of the 2D Brillouin zone. Equation (8) becomes

$$F_{ij}^{\kappa\kappa'}(\vec{q}_\perp) = \frac{1}{M}\sum_{\vec{n}'_\perp} F_{ij}(\vec{n}_\perp\kappa;\vec{n}'_\perp\kappa')e^{i\vec{q}_\perp\cdot[\vec{X}(\vec{n}'_\perp\kappa')-\vec{X}(\vec{n}_\perp\kappa)]}. \tag{21}$$

The coupling parameters F_{ij} are related to the force constants f_{ij} by relations similar to Eqs. (17a) and (17b). Notice that although the equilibrium positions of the A and B atoms are in a plane (X,Y), we allow for 3D displacements $u_i(\vec{n}_\perp\kappa)$,

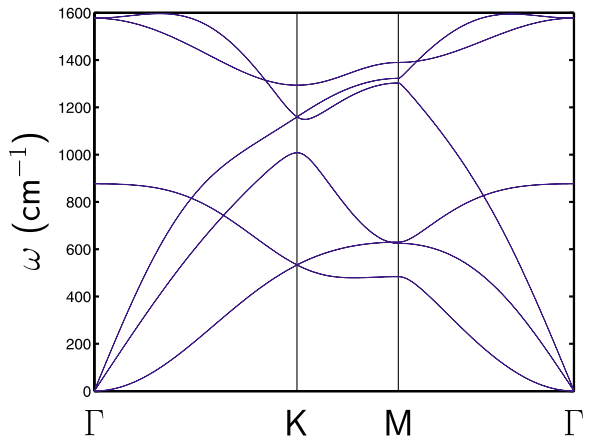

FIG. 3. (Color online) Phonon-dispersion relations of graphene, in agreement with Ref. 30.

where $i=x,y,z$. The dynamical matrix is conveniently written in terms of 3×3 submatrices $F^{\kappa\kappa'}(\vec{q}_\perp)$:

$$F(\vec{q}_\perp)=\begin{bmatrix} F^{AA}(\vec{q}_\perp) & F^{AB}(\vec{q}_\perp) \\ F^{BA}(\vec{q}_\perp) & F^{BB}(\vec{q}_\perp) \end{bmatrix}, \tag{22}$$

where the elements

$$F_{ij}^{AA}(\vec{q}_\perp)=\frac{1}{M}\left[\sum_{\vec{n}'_\perp\kappa'}{}' f_{ij}(\vec{n}_\perp A;\vec{n}'_\perp\kappa') - \sum_{\vec{n}'_\perp} f_{ij}(\vec{n}_\perp A;\vec{n}'_\perp A)e^{i\vec{q}_\perp\cdot[\vec{X}(\vec{n}'_\perp A)-\vec{X}(\vec{n}_\perp A)]}\right] \tag{23a}$$

are real while

$$F_{ij}^{AB}(\vec{q}_\perp)=-\frac{1}{M}\sum_{\vec{n}'_\perp} f_{ij}(\vec{n}_\perp A;\vec{n}'_\perp B)e^{i\vec{q}_\perp\cdot[\vec{X}(\vec{n}'_\perp B)-\vec{X}(\vec{n}_\perp A)]} \tag{23b}$$

are complex. One has the properties

$$F^{BB}(\vec{q}_\perp)=F^{AA}(\vec{q}_\perp), \tag{23c}$$

$$F^{BA}(\vec{q}_\perp)=F^{AB}(\vec{q}_\perp)^*. \tag{23d}$$

The force constants f_{ij} are symmetric in i and j, hence

$$F_{ij}^{\kappa\kappa'}=F_{ji}^{\kappa\kappa'}. \tag{23e}$$

In Appendix A we give expressions of the matrix elements $F_{ij}^{\kappa\kappa'}(\vec{q}_\perp)$, based on interatomic force constants up to fifth neighbors. The inclusion of fifth neighbors takes into account the long-range character of the intraplane valence forces in a (semi)metal such as graphene,[14,29] and improves overall agreement with INS,[4] IXS,[30] and high-resolution electron energy-loss spectroscopy[36] measurements of the phonon branches. Solution of the secular equation then leads to the phonon branches $\omega_\gamma(\vec{q})$, where $\gamma=1,\ldots,6$. In Fig. 3 we show the results of our calculation with force constants taken from Ref. 30; a comparison with experiments and *ab initio* calculations[4,14,29,37] is given in Ref. 30.

B. Graphite

In order to calculate the dynamical matrix of graphite, we have to distinguish between intraplane forces f_{ij}, described by the previous force constant model, and interplane van der Waals forces with force constants h_{ij}. We recall that the Brillouin zone is three dimensional. We write $\vec{q}_\perp$ for a vector with components $(q_1,q_2,0)$ and $\vec{q}$ for (q_1,q_2,q_3). The dynamical matrix $D(\vec{q})$ of dimension 12×12 is written in terms of 6×6 submatrices $D^{\alpha\alpha},D^{\beta\beta},\ldots$,

$$D(\vec{q})=\begin{bmatrix} D^{\alpha\alpha}(\vec{q}_\perp) & D^{\alpha\beta}(\vec{q}) \\ D^{\beta\alpha}(\vec{q}) & D^{\beta\beta}(\vec{q}_\perp) \end{bmatrix}. \tag{24}$$

Here the superscripts α and β refer to the two types of graphene planes. The submatrices are in turn expressed in terms of 3×3 intraplane and interplane submatrices $F^{\kappa\kappa'}(\vec{q}_\perp)$ and $H^{\kappa\kappa'}(\vec{q})$, respectively:

$$D^{\alpha\alpha}(\vec{q}_\perp)=\begin{bmatrix} 2H^{AA}+F^{AA}(\vec{q}_\perp) & F^{AB}(\vec{q}_\perp) \\ F^{BA}(\vec{q}_\perp) & 2H^{BB}+F^{BB}(\vec{q}_\perp) \end{bmatrix}, \tag{25a}$$

$$D^{\alpha\beta}(\vec{q})=\begin{bmatrix} H^{AA'}(\vec{q}) & H^{AB'}(\vec{q}) \\ H^{BA'}(\vec{q}) & H^{BB'}(\vec{q}) \end{bmatrix}, \tag{25b}$$

$$D^{\beta\beta}(\vec{q}_\perp)=\begin{bmatrix} 2H^{A'A'}+F^{A'A'}(\vec{q}_\perp) & F^{A'B'}(\vec{q}_\perp) \\ F^{B'A'}(q_\perp) & 2H^{B'B'}+F^{B'B'}(\vec{q}_\perp) \end{bmatrix}. \tag{25c}$$

In addition to the properties [Eqs. (23c)–(23e)], one has, as a consequence of crystal structure,

$$F^{A'A'}(\vec{q}_\perp)=F^{B'B'}(\vec{q}_\perp)=F^{AA}(\vec{q}_\perp), \tag{26a}$$

$$F^{A'B'}(\vec{q}_\perp)=F^{AB}(\vec{q}_\perp)^*. \tag{26b}$$

The numerical values of the intraplane matrix elements are the same as for the case of graphene (Appendix A).

The interplane elements read

$$H_{ij}^{\kappa\kappa'}(\vec{q})=-\frac{1}{M}\sum_{\vec{n}'\kappa'} h_{ij}(\vec{n}\kappa;\vec{n}'\kappa')e^{i\vec{q}\cdot[\vec{X}(\vec{n}'\kappa)-\vec{X}(\vec{n}\kappa)]}. \tag{27}$$

The matrices $H^{AA}=H^{A'A'}$ and $H^{BB}=H^{B'B'}$ are diagonal with real elements

$$H_{ii}^{AA}=-\frac{1}{2}[H_{ii}^{AA'}(\vec{q}=\vec{0})+H_{ii}^{AB'}(\vec{q}=\vec{0})], \tag{28a}$$

$$H_{ii}^{BB}=-\frac{1}{2}[H_{ii}^{BA'}(\vec{q}=\vec{0})+H_{ii}^{BB'}(\vec{q}=\vec{0})]. \tag{28b}$$

We quote the properties

$$H^{AA'}(\vec{q})=H^{A'A}(\vec{q}), \tag{29a}$$

TABLE I. Normalized optical eigenvectors $w^{(\lambda)}(\kappa i)$ and corresponding eigenfrequencies ω_λ for graphite in units of cm^{-1}.

κ	$w^{(1)}$	$w^{(2)}$	$w^{(3)}$	$w^{(4)}$	$w^{(5)}$	$w^{(6)}$	$w^{(7)}$	$w^{(8)}$	$w^{(9)}$
	$\frac{1}{2}$	0	0	0	0	$\frac{1}{2}$	0	0	$\frac{1}{2}$
A	0	$\frac{1}{2}$	0	0	0	0	$\frac{1}{2}$	$-\frac{1}{2}$	0
	0	0	$-\frac{1}{2}$	$\frac{1}{2}$	$\frac{1}{2}$	0	0	0	0
	$\frac{1}{2}$	0	0	0	0	$-\frac{1}{2}$	0	0	$-\frac{1}{2}$
B	0	$\frac{1}{2}$	0	0	0	0	$-\frac{1}{2}$	$\frac{1}{2}$	0
	0	0	$-\frac{1}{2}$	$-\frac{1}{2}$	$-\frac{1}{2}$	0	0	0	0
	$-\frac{1}{2}$	0	0	0	0	$\frac{1}{2}$	0	0	$-\frac{1}{2}$
A'	0	$-\frac{1}{2}$	0	0	0	0	$\frac{1}{2}$	$\frac{1}{2}$	0
	0	0	$\frac{1}{2}$	$\frac{1}{2}$	$-\frac{1}{2}$	$\frac{1}{2}$	0	0	0
	$-\frac{1}{2}$	0	0	0	0	$-\frac{1}{2}$	0	0	$\frac{1}{2}$
B'	0	$-\frac{1}{2}$	0	0	0	0	$-\frac{1}{2}$	$-\frac{1}{2}$	0
	0	0	$\frac{1}{2}$	$-\frac{1}{2}$	$\frac{1}{2}$	0	0	0	0
ω_λ	43.00	43.00	127.52	880.78	881.72	1577.20	1577.20	1577.54	1577.54
Γ	E_{2g_1}	E_{2g_1}	B_{2g_1}	A_{2u}	B_{2g_2}	E_{1u}	E_{1u}	E_{2g_2}	E_{2g_2}

$$H^{BB'}(\vec{q}) = H^{B'B}(\vec{q})^*, \tag{29b}$$

$$H^{BA'}(\vec{q}) = H^{AB'}(\vec{q}). \tag{29c}$$

Finally, we have $D^{\alpha\beta}(\vec{q}) = D^{\beta\alpha}(q)^*$ and $D^{\beta\beta}(\vec{q}) = D^{\alpha\alpha}(\vec{q})^*$. The presence of the $\vec{q}$-independent terms $2H^{AA}$ and $2H^{BB}$ (also called self-interactions) in the expression of $D^{\alpha\alpha}(\vec{q}_\perp)$ accounts for the fact that the neighboring β planes at $z = \pm c/2$ lead to an Einstein potential for the A and B atoms of the given α plane. A similar role is played by $2H^{A'A'}$ and $2H^{B'B'}$ in $D^{\beta\beta}(\vec{q}_\perp)$.

We now turn to the computation of interactions between layers. A straightforward way to obtain values of the interplane force constants $h_{ij}(\vec{n}\kappa;\vec{n}'\kappa')$ is to start from an empirical LJ potential between C atoms in different planes:

$$V(r) = \frac{\mathcal{B}}{r^{12}} - \frac{\mathcal{A}}{r^6}, \tag{30}$$

where $r = |\vec{X}(n\kappa) - \vec{X}(\vec{n}'\kappa')|$ is the equilibrium interatomic distance. For graphene-graphene interactions, the values $\mathcal{B} = 24.1 \times 10^3$ eV Å^{12} and $\mathcal{A} = 15.2$ eV Å^6 have been suggested.[35] We have calculated the force constants and the corresponding elements $H_{ij}^{\kappa\kappa'}(\vec{q})$ in Appendix B. Subsequently we calculated the nine optical zone-center modes of graphite by diagonalizing the dynamical matrix $D(\vec{q}=\vec{0})$. We recall that the decomposition into irreducible representations reads[8,7] $\Gamma = A_{2u} + 2B_{2g} + E_{1u} + 2E_{2g}$. We obtained fair values of seven of the optical mode eigenfrequencies; however the value 19.88 cm^{-1} of the degenerate shear type rigid layer mode frequency $\omega(E_{2g_1})$ is small in comparison with the value 42 ± 1 cm^{-1} from Raman-scattering experiments.[38] An attempt to increase the value of the LJ attraction parameter $\mathcal{A}$ leads to a concomitant strong decrease in the out-of-plane rigid layer mode frequency $\omega(B_{2g}) \approx 130$ cm^{-1} and hence is not allowed; a decrease in the repulsion parameter $\mathcal{B}$ leads to a similar failure. An analytical expression of $\omega(E_{2g_1})$ is readily obtained by hand:

$$\omega(E_{2g_1}) = \{-[H_{11}^{AA'}(\vec{q}=\vec{0}) + H_{11}^{BB'}(\vec{q}=\vec{0}) + H_{11}^{AB'}(\vec{q}=\vec{0}) + H_{11}^{AB'}(\vec{q}=\vec{0})]\}^{1/2}. \tag{31}$$

Using the force-constant parameters from Table V and Appendix B, we realize that the low numerical value of $\omega(E_{2g_1})$ is essentially due to the large negative value $h_{11}(0;1_+) = -114.47$ dyn/cm of the nearest-neighbor $A-A'$ force constant. We conclude that the interplane nearest-neighbor LJ potential is not sufficient to describe adequately the shear forces between rigid graphene layers. This fact is not too surprising since the overlap between π electron wave functions belonging to neighboring $A-A'$ atoms gives rise to a relatively large tight-binding parameter γ_1 (γ_1'),[17–19,39,40] which determines the width of π bands at the K point of the Brillouin zone. We recall that the graphene-graphene LJ potential of Ref. 35 was originally designed to account for interlayer cohesive properties.[34] These properties are essentially governed by the interplanar force constant $h_{33}(0;1_+) = 2040.41$ dyn/cm between A and A' atoms (see Table V and Appendix B); therefore the LJ potential already accounts well for the B_{2g} out-of-plane vibrational mode (experimental value 127 cm^{-1}). Replacing the LJ values of $h_{11}(0;1_+)$ and $h_{33}(0;1_+)$ by the *ad hoc* values 400.00 and 1800.00 dyn/cm, respectively, results in the eigenfrequencies $\omega(E_{2g_1}) = 42.98$ cm^{-1} and $\omega(B_{2g_1}) = 127.52$ cm^{-1}. Diagonalization of the dynamical matrix $D(\vec{q}=\vec{0})$ then leads to the results shown in Table I. The obtained zone-center optical eigenfrequencies are reasonably close to the experimental values[4,7,38] although small differences remain for the highest frequency values. For instance, the value 1577.54 cm^{-1} for the E_{2g_2} mode differs from the experimental value 1582 cm^{-1} measured by Raman scattering.[38] However, this difference will not affect our calculations of the elastic properties (Secs. IV and V)

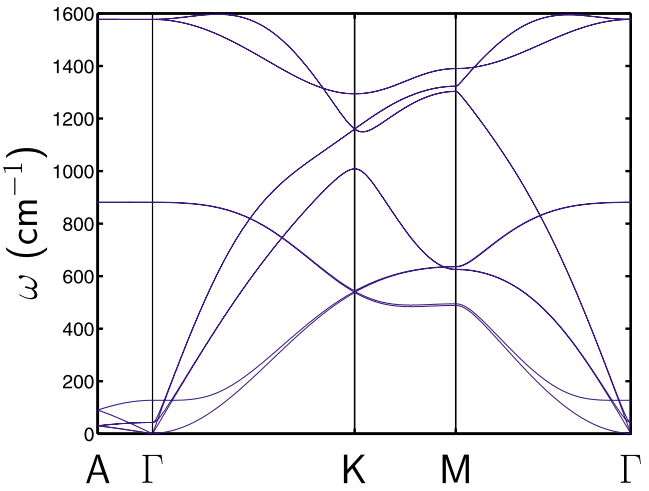

FIG. 4. (Color online) Phonon-dispersion relations of graphite along $A-\Gamma$ and in the $\Gamma-K-M$ basal plane.

since $(\omega_1)^{-2} \gg (\omega_9)^{-2}$ [see Eqs. (47) and (67a)].

The phonon spectrum of graphite (Fig. 4) is obtained by numerically solving the secular equation with the dynamical matrix $D(\vec{q})$ given by Eq. (24). In the basal plane of the Brillouin zone, the overall similarity of the graphite phonon spectrum with the six phonon branches of graphene is striking. Only at low energy near the Γ point do the weak interplane interactions cause a noticeable mode splitting. In particular the low-lying A_{2u} acoustic mode (characterized by atomic displacements normal to the plane) of the single layer splits up into an acoustic A_{2u} mode and an optical B_{2g} mode of graphite.[4,7] In Sec. VI we will consider this optical mode as the fingerprint of graphite when studying the evolution of the phonon spectrum of graphene multilayer slabs as a function of the layer number N. In Figs. 3 and 4 the highest optical phonon branches near the Γ and K points of the Brillouin zone are too flat in comparison with experimental results,[29,30] which show steeper slopes. The softening of the E_{2g} Γ point[37] and the A_1' K point modes[29] is attributed to strong electron-phonon coupling in sp^2 bonded carbon. These features have been identified and analyzed as Kohn anomalies.[41] In the following we study elastic properties which do not depend on the slope of the highest optical phonon branches.

IV. ELASTIC STRETCHING AND BENDING OF GRAPHENE

We first derive the elastic strain properties of graphene within the present lattice-dynamical model by applying Born's long-wave method to the 6×6 dynamical matrix $F(\vec{q}_\perp)$. In order to calculate the contributions $[ij,kl]$ and (ik,jl) to the dynamical matrix and to the elastic constants, we follow the steps summarized in Eqs. (10)–(15). We recall that neither A nor B atoms are centers of symmetry. The series expansion (10) now reads

$$F_{ij}^{\kappa\kappa'}(\vec{q}_\perp) = F_{ij}^{\kappa\kappa'(0)} + i\sum_k F_{ij,k}^{\kappa\kappa'(1)} q_k + \frac{1}{2}\sum_{kl} F_{ij,kl}^{\kappa\kappa'(2)} q_k q_l + \cdots . \tag{32}$$

The indices i (j) with values 1, 2, and 3 label the displacements in x, y, and z directions. The 2D wave vector $\vec{q}_\perp$ has the components (q_x, q_y) or equivalently (q_1, q_2). The expansion coefficients are obtained from the elements $F_{ij}^{\kappa\kappa'}(\vec{q}_\perp)$ in Appendix A. The quantities $[ij,kl]$ are then given by

$$[ij,kl]_{2D} = \frac{M}{2v_{2D}}\sum_{\kappa\kappa'} F_{ij,kl}^{\kappa\kappa'(2)}, \tag{33}$$

with $v_{2D}=a^2\sqrt{3}/2$ being the area of the 2D unit cell. One finds, in terms of the empirical force constants of Ref. 30 (see Table V in Appendix A),

$$[11,11]_{2D} = \frac{1}{4\sqrt{3}}\{[f_i^{(1)} + 3f_r^{(1)}] + 6[f_i^{(2)} + 3f_r^{(2)}] + 4[f_i^{(3)} + 3f_r^{(3)}] + 14[f_i^{(4)} + 3f_r^{(4)}] + 18[f_i^{(5)} + 3f_r^{(5)}]\}, \tag{34}$$

with $[22,22]_{2D}=[11,11]_{2D}$. The quantities $[11,22]_{2D}=[22,11]_{2D}$ are obtained from $[11,11]_{2D}$ by interchange of $f_i^{(n)}$ and $f_r^{(n)}$. Furthermore one has

$$[12,12]_{2D} = [21,21]_{2D} = \frac{1}{4\sqrt{3}}\{[f_r^{(1)} - f_i^{(1)}] + 6[f_r^{(2)} - f_i^{(2)}] + 4[f_r^{(3)} - f_i^{(3)}] + 14[f_r^{(4)} - f_i^{(4)}] + 18[f_r^{(5)} - f_i^{(5)}]\}, \tag{35}$$

while

$$[11,11]_{2D} - [11,22]_{2D} = 2[12,12]_{2D}. \tag{36}$$

We also quote $[11,12]_{2D}=[22,12]_{2D}=0$. Finally one has

$$[33,11]_{2D} = [33,22]_{2D} = \frac{1}{\sqrt{3}}[f_o^{(1)} + 6f_o^{(2)} + 4f_o^{(3)} + 14f_o^{(4)} + 18f_o^{(5)}], \tag{37}$$

and, since $q_3=0$, $[11,33]_{2D}=[22,33]_{2D}=[13,13]_{2D}=0$.

The quantities (ik,jl) [Eq. (13)], due to inner displacements, now read

$$(ik,jl)_{2D} = -(M/v_{2D})\sum_{\kappa\kappa'}\sum_{hp}\sum_{\kappa''\kappa'''}\Gamma_{hp}^{\kappa\kappa'} F_{hi,k}^{\kappa\kappa''(1)} F_{pj,l}^{\kappa'\kappa'''(1)}, \tag{38}$$

with

$$\Gamma_{hp}^{\kappa\kappa'} = \sum_{\lambda=1}^{3} \frac{w^{(\lambda)}(\kappa h) w^{(\lambda)}(\kappa' p)}{\omega_\lambda^2}, \tag{39}$$

where ω_λ and $w^{(\lambda)}$ are the optical phonon eigenfrequencies and eigenvectors of the dynamical matrix at $\vec{q}_\perp=\vec{0}$. We notice that only coefficients $F_{ij,k}^{\kappa\kappa'(1)}$ with $\kappa\neq\kappa'$ are nonzero. This property, which is a consequence of the crystal structure, implies that the quantities $(ik,jl)_{2D}$ account for the A-B sublattice shifts. Hermiticity of the dynamical matrix leads to

$$F_{ij,k}^{AB(1)} = -F_{ij,k}^{BA(1)}. \tag{40}$$

In addition, the 2D hexagonal crystal structure implies that elements with i,j or $k=3$ are zero. Furthermore, $F_{22,2}^{AB(1)} = F_{12,1}^{AB(1)} = F_{21,1}^{AB(1)} = F_{11,2}^{AB(1)} = 0$, while $F_{12,2}^{AB(1)} = F_{21,2}^{AB(1)} = F_{22,1}^{AB(1)} = -F_{11,1}^{AB(1)} \neq 0$. Explicitly we obtain

$$F_{11,1}^{AB(1)} = \frac{\sqrt{3}a}{4M}\Delta f_{ir}^{AB}, \tag{41}$$

where

$$\Delta f_{ir}^{AB} = \{f_i^{(1)} - f_r^{(1)} - 2[f_i^{(3)} - f_r^{(3)}] + s^{(4)}[f_i^{(4)} - f_r^{(4)}]\}, \tag{42}$$

with $s^{(4)}=5\cos 2\theta_1 - \sqrt{3}\sin 2\theta_1$, where $\theta_1 = \arctan(\sqrt{3}/5)$, i.e., numerically $s^{(4)} \approx 2.86$.

In order to calculate the optical phonon frequencies at the Γ point of the Brillouin zone, we introduce the three optical displacements vectors $w^{(1)}(\kappa i) = \sqrt{\frac{1}{2}}(1,0,0,-1,0,0)$, $w^{(2)}(\kappa i) = \sqrt{\frac{1}{2}}(0,1,0,0,-1,0)$, and $w^{(3)}(\kappa i) = \sqrt{\frac{1}{2}}(0,0,1,0,0,-1)$, and evaluate

$$\sum_{\kappa\kappa'}\sum_{ij} w^{(\lambda)}(\kappa i) F_{ij}^{\kappa\kappa'(0)} w^{(\mu)}(\kappa' j) = \omega_\lambda^2(\vec{q}=\vec{0})\delta_{\lambda\mu}, \tag{43}$$

obtaining

$$\omega_1^2(\vec{0}) = \omega_2^{(2)}(\vec{0}) = \frac{3}{M}\{[f_i^{(1)} + f_r^{(1)}] + [f_i^{(3)} + f_r^{(3)}] + 2[f_i^{(4)} + f_r^{(4)}]\}, \tag{44a}$$

$$\omega_3^2(\vec{0}) = \frac{6}{M}[f_o^{(1)} + f_o^{(3)} + 2f_o^{(4)}]. \tag{44b}$$

With the force constant values of Ref. 30, the optical phonon energies at $\vec{q}_\perp = \vec{0}$ are $\hbar\omega_1(\vec{0}) = \hbar\omega_2(\vec{0}) = 195.5$ meV and $\hbar\omega_3(\vec{0}) = 108.6$ meV, in agreement with Fig. 3. The elements of the 6×6 matrix Γ are

$$\Gamma_{\lambda\mu}^{AA} = \Gamma_{\lambda\mu}^{BB} = \frac{1}{2\omega_\lambda^2(\vec{0})}\delta_{\lambda\mu}, \tag{45a}$$

$$\Gamma_{\lambda\mu}^{AB} = \Gamma_{\lambda\mu}^{BA} = -\Gamma_{\lambda\mu}^{AA}. \tag{45b}$$

Using Eqs. (40), (45a), and (45b), we rewrite the inner displacement term [Eq. (38)] as

$$(ik,jl)_{2D} = -\frac{4M}{v_{2D}}\sum_{\lambda=1}^{2}\frac{1}{2\omega_\lambda^2(\vec{0})}F_{\lambda i,k}^{AB(1)}F_{\lambda j,l}^{AB(1)}. \tag{46}$$

In particular we find

$$(11,11)_{2D} = -\frac{\sqrt{3}(\Delta f_{ir}^{AB})^2}{4\omega_1^2(\vec{0})M}, \tag{47}$$

with $(22,22)_{2D} = (12,12)_{2D} = (11,11)_{2D} = -(11,22)_{2D} = -(22,11)_{2D}$.

The elastic constants that characterize the rigidity of the 2D crystal against in-plane deformations are obtained by means of Eq. (15). They are in fact surface-tension coefficients. We write $\Gamma_{ij,kl}$ instead of $C_{ij,kl}$ and γ_{ij} for c_{ij}. Using Voigt's notation, we find

$$\gamma_{11} \equiv \Gamma_{11,11} = [11,11]_{2D} + (11,11)_{2D}, \tag{48}$$

where $[11,11]_{2D}$ and $(11,11)_{2D}$ are given by Eqs. (34) and (47), respectively. Similarly we get

$$\gamma_{12} \equiv \Gamma_{11,22} = 2[12,12]_{2D} - [11,22]_{2D} + (11,22)_{2D}, \tag{49a}$$

$$\gamma_{66} \equiv \Gamma_{12,12} = [11,22]_{2D} + (12,12)_{2D}. \tag{49b}$$

One verifies by means of Eq. (36) that the relation $\gamma_{11} - \gamma_{12} = 2\gamma_{66}$, characteristic for a hexagonal crystal, is analytically fulfilled. The longitudinal and transverse sound velocities for in-plane displacements are given by $c_l = \sqrt{\gamma_{11}/\rho_{2D}}$ and $c_t = \sqrt{\gamma_{66}/\rho_{2D}}$, where $\rho_{2D} = \frac{2M}{v_{2D}} = 7.61\times 10^{-8}$ g/cm^2 is the surface mass density. With the values of the empirical force constants of Ref. 30, we obtain the numerical results (all in units of 10^4 dyn/cm): $[11,11]_{2D} = 47.28$, $[12,12]_{2D} = 12.45$, $[11,22]_{2D} = 22.38$, and $(11,11)_{2D} = -6.73$.

The (3×3) acoustic dynamical matrix in the long-wavelength limit is given by[31]

$$\hat{F}_{ij}(\vec{q}_\perp) = \frac{1}{\rho_{2D}}\sum_{kl}\{[ij,kl]_{2D} + (ik,jl)_{2D}\}q_k q_l. \tag{50}$$

Explicitly one has

$$\hat{F}_{11}(\vec{q}_\perp) = \frac{1}{\rho_{2D}}\{[(11,11)_{2D} + (11,11)_{2D}]q_1^2 + [(11,22)_{2D} + (12,12)_{2D}]q_2^2\}, \tag{51a}$$

where $\hat{F}_{22}(\vec{q}_\perp)$ is obtained from $\hat{F}_{11}(\vec{q}_\perp)$ by interchanging q_1 and q_2, where

$$\hat{F}_{12}(\vec{q}_\perp) = \hat{F}_{21}(\vec{q}_\perp) = \frac{2}{\rho_{2D}}[12,12]_{2D}q_1 q_2, \tag{51b}$$

$$\hat{F}_{33}(\vec{q}_\perp) = \frac{1}{\rho_{2D}}\{[33,11]_{2D}(q_1^2 + q_2^2)\}, \tag{51c}$$

$$\hat{F}_{j3}(\vec{q}_\perp) = \hat{F}_{3j}(\vec{q}_\perp) = 0, \quad j = 1,2. \tag{51d}$$

Numerical results of the present work, results from first-principles density-functional calculations[37] of a single graphite layer, as well as results from full in-plane IXS on single-crystalline graphite[28] are summarized in Table II. We observe that the inner displacement terms $(ij,kl)_{2D}$ give quantitatively important contributions to the values of the tension coefficients obtained by the present theory. From Eq. (51a) of the acoustic dynamical matrix $\hat{F}_{11}(\vec{q}_\perp)$, it follows that the inner displacement terms are also comprised in the in-plane longitudinal and transverse sound velocities $c_l \equiv V(\mathrm{LA}[100]_{\langle 100\rangle})$ and $c_t \equiv V(\mathrm{LA}[100]_{\langle 1\bar{2}0\rangle})$, respectively. Here the numbers within [ ] brackets refer to the propagation

TABLE II. Elastic stiffness (tension) coefficients (units of 10^4 dyn/cm) and sound velocities (units in km/s) of graphene.

	γ_{11}	γ_{66}	c_l	c_t
Present theory	40.5	15.66	23.08	14.34
First principles results (Ref. 37)	38.5,[a]51.5[b]	19.5[c]	26.0	16.0
IXS in-plane (graphite) (Ref. 28)	37.37[d]	16.35[d]	22.16	14.66

[a]Elastic stiffness of 63 eV/atom.
[b]From $c_l=26$.
[c]From $c_t=16$.
[d]Derived from $c_l=22.16$ and $c_t=14.66$.

wave vector and the numbers within $\langle\ \rangle$ brackets refer to the polarization of displacements. Our values of c_l and c_t are in close agreement with V(LA) and V(TA), respectively, of Ref. 28; hence we conclude that, in agreement with the interpretation of the experimental results of phonon dispersions in Ref. 30, V(LA) and V(TA) refer to phonons of a single graphene sheet.

Within the present force-constant model,[30] we obtain from Eq. (37) that $[33,11]_{2D}=-0.0175\times10^4$ dyn/cm, which means that $[33,11]_{2D}$ is numerically negligible in comparison with $[11,22]_{2D}$, etc.. Strictly speaking, symmetry requires that the elastic energy density of a thin plate should not contain a second-order gradient term in the out-of-plane displacements.[42] Hence we conclude that $[33,11]_{2D}$ should be identically zero. This can be achieved by a slight increase in the force-constant model parameter $f_o^{(5)}$ (using a value of 0.112 eV/Å^2 instead of 0.110 eV/Å^2). Such a change does not affect, in any noticeable way, the phonon-dispersion relations (Fig. 3).

Within the present model, there is no coupling between the in-plane and the out-of-plane acoustic displacements. The elastic energy per unit surface is obtained from

$$U_{2D}=\lim_{\vec{q}_\perp\to0}\frac{1}{2S}\sum_{ij}s^\dagger(\vec{q}_\perp)\hat{F}_{ij}(\vec{q}_\perp)s_j(\vec{q}_\perp), \tag{52}$$

where $S=N_{2D}v_{2D}$ with N_{2D} as the number of unit cells in the graphene plane. Here we have introduced the acoustic displacements

$$s_i(\vec{q}_\perp)=\frac{1}{\sqrt{2}}[u_i^A(\vec{q}_\perp)+u_i^B(\vec{q}_\perp)], \tag{53}$$

which account for center-of-mass displacements of the unit cells. It is convenient to separate the elastic energy into a part U_i due to in-plane displacements, i.e., s_1 and s_2 components, and a term U_o due to out-of-plane displacements, i.e., s_3: $U_{2D}=U_i+U_o$. Defining homogeneous strains for in-plane displacements

$$\varepsilon_{ij}=\lim_{\vec{q}_\perp\to\vec{0}}\frac{1}{2\sqrt{MN_{2D}}}[q_is_j(\vec{q}_\perp)+q_js_i(\vec{q}_\perp)], \tag{54}$$

we find from Eqs. (48)–(50), (51a), (52), and (53) that

$$U_i=\frac{1}{2}[\gamma_{11}(\varepsilon_{11}^2+\varepsilon_{22}^2)+2\gamma_{12}\varepsilon_{11}\varepsilon_{22}+2(\gamma_{11}-\gamma_{12})\varepsilon_{12}^2]. \tag{55a}$$

The rigidity of graphene against in-plane deformations is characterized by the two elastic constants γ_{11} and γ_{12}. Using $\gamma_{11}-\gamma_{12}=2\gamma_{66}$, we rewrite U_i as

$$U_i=\frac{1}{2}\{(\gamma_{11}-\gamma_{66})(\varepsilon_{11}+\varepsilon_{22})^2+\gamma_{66}[(\varepsilon_{11}-\varepsilon_{22})^2+4\varepsilon_{12}^2]_{2D}\}. \tag{55b}$$

We then identify $\gamma_{11}-\gamma_{66}=B_{2D}=24.89\times10^4$ dyn/cm, and $\gamma_{66}=\mu_{2D}$ with the bulk modulus and the shear modulus, respectively, while $\gamma_{12}=\lambda_{2D}$ plays the role of Lamé coefficient. We recall[42] that for a 2D hexagonal solid $B_{2D}=\lambda_{2D}+\mu_{2D}$. We notice that B_{2D} and μ_{2D} are positive as is required by thermodynamic stability.[43] Since the elastic properties of a 2D hexagonal crystal are isotropic in the crystal plane,[42] we use the expressions of Young's modulus and Poisson's ratio for a 2D isotropic solid:[44]

$$Y_{2D}=\frac{4B_{2D}\mu_{2D}}{B_{2D}+\mu_{2D}}, \tag{56a}$$

$$\sigma_{2D}=\frac{B_{2D}-\mu_{2D}}{B_{2D}+\mu_{2D}}. \tag{56b}$$

We obtain the values $Y_{2D}=38.46\times10^4$ dyn/cm and $\sigma_{2D}=0.228$, respectively. We note that our value for B_{2D} is much larger than the value 0.4 eV Å^{-2} quoted in Ref. 27 and derived from an effective many-body carbon potential.

In order to study the bending energy of the 2D crystal, we expand the elements $F_{33}^{\kappa\kappa'}(\vec{q}_\perp)$ of the dynamical matrix up to fourth order in the wave-vector components. The contribution to the acoustic dynamical matrix is found to be

$$\hat{F}_{33}^{(4)}(\vec{q}_\perp)=\kappa a^4(q_x^2+q_y^2)^2, \tag{57}$$

where

$$\kappa=-\frac{1}{192}[f_o^{(1)}+18f_o^{(2)}+16f_o^{(3)}+98f_o^{(4)}+162f_o^{(5)}]. \tag{58}$$

With the values of the force-constant parameters $f_o^{(n)}$ taken from Ref. 30, we obtain $\kappa=0.256\times10^4$ dyn/cm. The negative value of the fourth-neighbors force constant $f_o^{(4)}$ gives the main contribution to a positive value of κ. Writing

$\zeta(\vec{q}_\perp) \equiv s_3(\vec{q}_\perp)$ for the Fourier components of the acoustic out-of-plane displacements, we define the corresponding elastic energy per unit cell

$$U_b = \frac{1}{2S}\sum_{\vec{q}_\perp} \zeta^\dagger(\vec{q}_\perp)\hat{F}^{(4)}_{33}(\vec{q}_\perp)\zeta(\vec{q}_\perp). \tag{59}$$

In real space we obtain in the continuum limit

$$U_b = \frac{\tilde{\kappa}_b}{2N_c}\int\int dx_1 dx_2 [\nabla^2_\perp \zeta(x_1,x_2)]^2. \tag{60}$$

Here we have considered the out-of-plane displacements ζ as functions of the coordinates in the (x_1,x_2) plane and $\nabla^2_\perp = (\partial^2/\partial x_1^2 + \partial^2/\partial x_2^2)$. The right-hand side of Eq. (60) has the form of a bending energy, and is familiar from the theory of bending of thin plates[42] and membranes.[44] In the present case the bending rigidity $\tilde{\kappa}_b = 2\kappa a^2/\sqrt{3}$ is determined by the atomic force constants $f_o^{(n)}$ and the interatomic distances of the graphene crystal. We obtain $\tilde{\kappa}_b = 1.79\times 10^{-12}$ erg$=1.29\times 10^4$ Kelvin≈ 1.12 eV, which is in agreement with the value 1.1 eV obtained by atomistic Monte Carlo simulations.[27]

Within the present harmonic lattice dynamics theory, there is no coupling between in-plane and out-of-plane deformations. Hence a treatment of the anomalous elasticity effects due to the coupling between stretching and bending, as occurs in the theory of strongly bend plates[42] and in polymerized membranes,[45] is beyond the scope of the present work.

V. ELASTIC CONSTANTS OF GRAPHITE

There are five different elastic constants for graphite, i.e., $c_{11} \equiv C_{11,11}$, $c_{12} \equiv C_{11,22}$, $c_{13} \equiv C_{11,33}$, $c_{33} \equiv C_{33,33}$, and $c_{44} \equiv C_{23,23}$. One also considers $c_{66} = C_{12,12}$, where, due to hexagonal symmetry, $c_{11} - c_{12} = 2c_{66}$. We start from Eq. (15) and apply Born's long-wave method (Sec. II) using the $\vec{q}$ expansion of the dynamical matrix $D(\vec{q})$ [Eq. (24)]. We first calculate the square brackets $[ij,kl]$, defined by Eq. (12). Separating in the sums over atoms κ and κ' intraplane and interplane contributions, we write

$$[ij,kl] = [ij,kl]_{\alpha\alpha} + [ij,kl]_{\beta\beta} + 2[ij,kl]_{\alpha\beta}, \tag{61}$$

where

$$[ij,kl]_{\alpha\alpha} = \frac{M}{2v_c}\sum_{\kappa,\kappa'} F^{\kappa\kappa'(2)}_{ij,kl}, \quad \kappa,\kappa' \in \{A,B\}, \tag{62a}$$

$$[ij,kl]_{\alpha\beta} = \frac{M}{2v_c}\sum_{\kappa,\kappa'} H^{\kappa\kappa'(2)}_{ij,kl}, \quad \kappa \in A,B, \quad \kappa' \in \{A',B'\}, \tag{62b}$$

where $\{A,B\} \in \alpha$ plane and $\{A',B'\} \in \beta$ plane. Here the second-order coefficients $F^{\kappa\kappa'(2)}_{ij,kl}$ and $H^{\kappa\kappa'(2)}_{ij,kl}$ are obtained from a series expansion of the 3×3 matrices $F^{\kappa\kappa'}(\vec{q})$ and $H^{\kappa\kappa'}$ in powers of $\vec{q}$ [see Eq. (10)]. One has $[ij,kl]_{\alpha\alpha} = [ij,kl]_{\beta\beta}$ and $[ij,kl]_{\alpha\beta} = [ij,kl]_{\beta\alpha}$. Since $v_c = ca^2\sqrt{3}/2 = cv_{2D}$, we get

TABLE III. Quantities $[ij,kl]_{\alpha\alpha}$ and $[ij,kl]_{\alpha\beta}$; Σ stands for sum [Eq. (61)]. All results in units of 10^9 dyn/cm^2.

	$\alpha\alpha$	$\alpha\beta$	Σ
[11,11]	7056	1.57	14 115
[11,22]	3341	0.47	6682
[12,12]	1858	0.56	3717
[22,33]	0	20.91	41.82
[33,22]	0	11.80	23.60
[13,13]	0	11.92	23.85
[33,33]	0	183.92	367.86

$$[ij,kl]_{\alpha\alpha} = [ij,kl]_{\beta\beta} = \frac{1}{c}[ij,kl]_{2D}, \tag{63}$$

where $[ij,kl]_{2D}$ is the corresponding quantity that has been calculated in Sec. IV for 2D graphene. Notice that $[ij,kl]_{\alpha\alpha}$ has the dimensions of dyn/cm^2, i.e. of 3D elastic constants. Hexagonal symmetry implies $[11,22]=[22,11]$, $[11,33]=[22,33]$, and $[33,22]=[33,11]$. Numerical values of $[ij,kl]_{\alpha\alpha}$ are quoted in Table III. We rewrite the interplane term as

$$[ij,kl]_{\alpha\beta} = \frac{M}{ca^2\sqrt{3}}[H^{AA'(2)}_{ij,kl} + H^{BB'(2)}_{ij,kl} + 2H^{AB'(2)}_{ij,kl}], \tag{64}$$

where we have used $H^{AB'(2)}_{ij,kl} = H^{BA'(2)}_{ij,kl}$. The coefficients $H^{\kappa\kappa'(2)}_{ij,kl}$ are obtained as second-order terms from a $\vec{q}$ expansion of the matrix elements $H^{\kappa\kappa'}_{ij}(\vec{q})$; they are linear combinations of the interplane force constants $h_{ij}(\vec{n}\kappa;\vec{n}'\kappa')$ given in Appendix B and Table V. Numerical results of the quantities $[ij,kl]_{\alpha\beta}$ are quoted in Table III.

For the calculation of the contributions (ij,kl) due to sublattice shifts to the elastic constants, one starts from the definition [Eq. (13)], which now reads

$$(ik,jl) = -\frac{M}{v_c}\sum_{\kappa\kappa'}\sum_{hp}\sum_{\kappa''\kappa'''} \Gamma^{\kappa\kappa'}_{hp} D^{\kappa\kappa''(1)}_{hi,k} D^{\kappa'\kappa'''(1)}_{pj,l}. \tag{65}$$

Separating the sums over κ and κ' atoms into intraplane and interplane contributions, we write

$$(ik,jl) = 2(ik,jl)_{\alpha\alpha} + 2(ik,jl)_{\alpha\beta}, \tag{66}$$

where we have used $(ik,jl)_{\alpha\alpha} = (ik,jl)_{\beta\beta}$ and $(ik,jl)_{\alpha\beta} = (ik,jl)_{\beta\alpha}$. In the following it suffices to calculate (11,11) since, by symmetry, $(11,11)=(22,22)=(12,12)=-(11,22)=-(22,11)$ while $(13,13)=(33,33)=(11,33)=0$.

Knowledge of the optical phonon eigenfrequencies and eigenvectors from Table I allows us to construct the elements $\Gamma^{\kappa\kappa'}_{ij}$ by means of Eq. (14). In particular we will need

$$\Gamma^{AA}_{11} = \frac{1}{4}\left[\frac{1}{(\omega_1)^2} + \frac{1}{(\omega_6)^2} + \frac{1}{(\omega_9)^2}\right], \tag{67a}$$

$$\Gamma^{AB}_{11} = \frac{1}{4}\left[\frac{1}{(\omega_1)^2} - \frac{1}{(\omega_6)^2} - \frac{1}{(\omega_9)^2}\right], \tag{67b}$$

$$\Gamma_{11}^{AA'} = \frac{1}{4}\left[-\frac{1}{(\omega_1)^2} + \frac{1}{(\omega_6)^2} - \frac{1}{(\omega_9)^2} \right], \tag{67c}$$

$$\Gamma_{11}^{AB'} = \frac{1}{4}\left[-\frac{1}{(\omega_1)^2} - \frac{1}{(\omega_6)^2} + \frac{1}{(\omega_9)^2} \right]. \tag{67d}$$

The first-order expansion coefficients $D_{ij,k}^{\kappa\kappa'(1)}$ are obtained readily from $D(\vec{q})$ in terms of elements $F_{ij,k}^{\kappa\kappa'(1)}$ and $H_{ij,k}^{\kappa\kappa'(1)}$. We quote the 12×12 matrix in terms of 3×3 submatrices:

$$(D_{ij,k}^{\kappa\kappa'(1)}) = \begin{bmatrix} 0 & F_{..,k}^{AB(1)} & 0 & H_{..,k}^{AB'(1)} \\ -F_{..,k}^{AB(1)} & 0 & H_{..,k}^{AB'(1)} & -H_{..,k}^{AB'(1)} \\ 0 & -H_{..,k}^{AB'(1)} & 0 & -F_{..,k}^{AB(1)} \\ -H_{..,k}^{AB'(1)} & H_{..,k}^{AB'(1)} & F_{..,k}^{AB(1)} & 0 \end{bmatrix}, \tag{68}$$

where $k=1,2$ with

$$F_{..,1}^{AB(1)} = \begin{bmatrix} F_{11,1}^{AB(1)} & 0 & 0 \\ 0 & -F_{11,1}^{AB(1)} & 0 \\ 0 & 0 & 0 \end{bmatrix}, \tag{69a}$$

$$F_{..,2}^{AB(1)} = \begin{bmatrix} 0 & -F_{11,1}^{AB(1)} & 0 \\ -F_{11,1}^{AB(1)} & 0 & 0 \\ 0 & 0 & 0 \end{bmatrix}. \tag{69b}$$

The submatrices $H_{..,k}^{AB'(1)}$ have the same structure as $F_{..,k}^{AB(1)}$ with $F_{11,1}^{AB(1)}$ replaced everywhere by $H_{11,1}^{AB'(1)}$. The element $F_{11,1}^{AB(1)}$ is given by Eq. (41) while $H_{11,1}^{AB'(1)}$ is obtained by expansion of $H_{11}^{AB'}(\vec{q})$ [Eq. (B4a)] in powers of small $\vec{q}$:

$$H_{11,1}^{AB'(1)} = \frac{2a}{\sqrt{3}M}[h_{11}(0;1'_+) - h_{11}(0;2'_+)]. \tag{70}$$

Taking into account the structure of the 12×12 matrices Γ and $D_{..,1}^{(1)}$, and carrying out the sums κ'' and κ''', we find

$$(11,11)_{\alpha\alpha} = S_{\alpha\alpha}^{FF} + S_{\alpha\alpha}^{HF} + S_{\alpha\alpha}^{HH}, \tag{71}$$

where

$$S_{\alpha\alpha}^{FF} = -\frac{2M}{v_c}(F_{11,1}^{AB})^2(\Gamma_{11}^{AA} - \Gamma_{11}^{AB}), \tag{72a}$$

$$S_{\alpha\alpha}^{HF} = -\frac{2M}{v_c}F_{11,1}^{AB}H_{11,1}^{AB'}(\Gamma_{11}^{AA} - \Gamma_{11}^{AB}), \tag{72b}$$

$$S_{\alpha\alpha}^{HH} = -\frac{M}{v_c}(H_{11,1}^{AB'})^2\Gamma_{11}^{AA}. \tag{72c}$$

Numerical evaluation gives $S_{\alpha\alpha}^{FF}=-100.4\times10^{10}$ dyn/cm^2, $S_{\alpha\alpha}^{FH}=-0.31\times10^{10}$ dyn/cm^2, and $S_{\alpha\alpha}^{HH}=-1.6\times10^{7}$ dyn/cm^2. Similarly we calculate

$$(11,11)_{\alpha\beta} = S_{\alpha\beta}^{FF} + S_{\alpha\beta}^{HF} + S_{\alpha\beta}^{HH}, \tag{73}$$

where

$$S_{\alpha\beta}^{FF} = -\frac{2M}{v_c}(F_{11,1}^{AB})^2(\Gamma_{11}^{AB'} - \Gamma_{11}^{AA'}), \tag{74a}$$

$$S_{\alpha\beta}^{HF} = -\frac{2M}{v_c}F_{11,1}^{AB}H_{11,1}^{AB'}(\Gamma_{11}^{AB'} - \Gamma_{11}^{AA'}), \tag{74b}$$

$$S_{\alpha\beta}^{HH} = +\frac{M}{v_c}(H_{11,1}^{AB'})^2\Gamma_{11}^{AA'}, \tag{74c}$$

and numerically $S_{\alpha\beta}^{FF}=2.2\times10^{8}$ dyn/cm^2, $S_{\alpha\beta}^{HF}=-6.8\times10^{5}$ dyn/cm^2, and $S_{\alpha\beta}^{HH}=-1.6\times10^{7}$ dyn/cm^2. Hence $(11,11)_{\alpha\beta}$ is numerically negligible. Retaining only $S_{\alpha\alpha}^{FF}$ and $S_{\alpha\alpha}^{FH}$, we obtain $(11,11)=2(S_{\alpha\alpha}^{FF}+S_{\alpha\alpha}^{FH})=-200.2\times10^{10}$ dyn/cm^2 for the inner displacement term.

The elastic constants of graphite are then given by

$$c_{11} = [11,11] + (11,11), \tag{75a}$$

$$c_{12} = 2[12,12] - [11,22] - (11,11), \tag{75b}$$

$$c_{66} = [11,22] + (11,11), \tag{75c}$$

$$c_{33} = [33,33]. \tag{75d}$$

We notice that the Huang conditions are not satisfied for $[22,33]\neq[33,22]$ (see Table III); however we assume

$$c_{44} = [22,33], \tag{76a}$$

$$c_{13} = 2[13,13] - [11,33]. \tag{76b}$$

The bulk modulus is given by[46]

$$B = \frac{c_{33}(c_{11}+c_{12}) - 2c_{13}^2}{(c_{11}+c_{12}) + 2c_{33} - 4c_{13}}. \tag{77}$$

With the numerical values of the quantities $[ij,kl]$ taken from Table III and $(11,11)=-200.2\times10^{10}$ dyn/cm^2, we obtain the values of the elastic constants and of the bulk modulus quoted in Table IV. Note that the identity $c_{11}-c_{12}=2c_{66}$ is satisfied. The longitudinal and transverse sound velocities are given by $c_l=\sqrt{c_{11}/\rho}$ and $c_t=\sqrt{c_{66}/\rho}$, where $\rho=\frac{4M}{v_c}$ is the mass density.

The agreement between the present theoretical values of the elastic constants and various experimental values, in particular recent single-crystal IXS results,[28] is remarkable. Our values of c_{11} and c_{66} differ by less than 10% from the corresponding single-crystal IXS values; we also draw attention to the small value of c_{13} where we agree with IXS. Agreement with earlier experimental results is hampered by the fact that the basic material was pyrolytic graphite.[4,5,12] Also the agreement with several *ab initio* calculations[15,49] is very satisfactory. As in the case of graphene, we find that the inner displacement terms give quantitative important contributions to the elastic constants.

It is possible to establish approximate relations between the elastic constants c_{11} and c_{66} of graphite, and the tension coefficients γ_{11} and γ_{66}, respectively, of graphene. We observe that the interplane terms $[ij,kl]_{\alpha\beta}$ are small in comparison with the intraplane terms $[ij,kl]_{\alpha\alpha}$ contributing to c_{11} and

TABLE IV. Elastic constants of graphite (units of GPa=10^{10} dyn/cm^2) and sound velocities (units in km/s).

	c_{11}	c_{12}	c_{66}	c_{33}	c_{44}	c_{13}	B	c_l	c_t
Present theory	1211.3	275.5	468.0	36.79	4.18	0.59	35.1	22.99	14.29
Experiment	1060(16)[a]	180(20)[a]	440(20)[a]	36.5(10)[a]	4.0(4)[a]	15(5)[a]			
	1440(20)[b]		460[b]	37.1(5)[b]	4.6(2)[b]				
	1109(16)[c]	139(36)[c]	485(10)[c]	38.7(7)[c]	5.0(3)[c]	0(3)[c]	36.4(11)[c]		
					5.05(35)[d]				
							33.8(30)[e]		
Ab initio	1118[f]	235[f]	441.5[f]	29.5[f]	4.5[f]				
	$c_{11}+c_{12}=1280$ [g]			40.8[g]					

[a]Ultrasonics and static tests (Refs. 5 and 12).
[b]Inelastic neutron scattering (Ref. 4).
[c]Inelastic x rays (Ref. 28).
[d]Brillouin scattering (Ref. 47).
[e]X-ray diffraction (Ref. 48).
[f]From LDA *ab initio* phonon dispersions (Ref. 49).
[g]*Ab initio* calculations (Ref. 15).

c_{66}. Hence we neglect the last term on the right-hand side of Eq. (61) and, by means of Eq. (63), we have approximately

$$[11,11] \approx \frac{2}{c}[11,11]_{2D}, \tag{78}$$

$$[11,22] \approx \frac{2}{c}[11,22]_{2D}. \tag{79}$$

We also notice that the last term on the right-hand side of Eq. (67c) is negligible, hence $(11,11) \approx 2(11,11)_{\alpha\alpha}$. In addition we neglect $S^{HF}_{\alpha\alpha}$ and $S^{HH}_{\alpha\alpha}$ on the right-hand side of Eq. (71). We also notice that the optical mode frequency $\omega_1(\vec{0}) = 1564\ \text{cm}^{-1}$ in graphene is close to the optical modes $\omega_6(\vec{0})$ and $\omega_9(\vec{0})$ of graphite. Hence we obtain from Eqs. (66), (71), (67a), (67b), and (47) the approximate relation

$$(11,11) \approx \frac{2}{c}(11,11)_{2D}, \tag{80a}$$

and similarly

$$(11,22) \approx \frac{2}{c}(11,22)_{2D}. \tag{80b}$$

From the definitions of the elastic constants [Eqs. (75a) and (75c)] and of the corresponding tension coefficients [Eqs. (48) and (49b)], we then obtain the approximate relations

$$c_{11} \approx \frac{2}{c}\gamma_{11}, \tag{81a}$$

$$c_{66} \approx \frac{2}{c}\gamma_{66}. \tag{81b}$$

Using the fact that $\rho = \frac{2}{c}\rho_{2D}$, we obtain the equality of the sound velocities:

$$c_l = \sqrt{\frac{c_{11}}{\rho}} \approx \sqrt{\frac{\gamma_{11}}{\rho_{2D}}}, \tag{82a}$$

$$c_t = \sqrt{\frac{c_{66}}{\rho}} \approx \sqrt{\frac{\gamma_{66}}{\rho_{2D}}}. \tag{82b}$$

Indeed from the numerical values for c_l and c_t in Tables II and IV, we see that the corresponding values for graphene and graphite are close to the experimental values from single-crystal in-plane IXS results.[28]

Finally a comment on turbostratic graphite is in order. The elastic constants c_{11}, c_{66}, and c_{12} are essentially determined by the intraplane force constants while the elastic constants c_{13}, c_{33}, and c_{44} are determined solely by interplane forces (see Table III). Hence we expect that, in turbostratic graphite (where adjacent basal planes are randomly rotated with respect to one another[50]), the values of the elastic constants c_{13}, c_{33}, and c_{44} are more drastically changed (in comparison with those of pyrolytic graphite) than c_{11}, c_{12}, and c_{66}. This is indeed the case.[50,51]

VI. GRAPHENE MULTILAYERS

Here we use the lattice-dynamical model of intraplane covalent force constants and interplane van der Waals forces (Sec. III) to investigate the phonon spectra of graphene multilayers, also called graphite slabs. The main aim of early work on graphite slabs has been the study of surface modes.[52] Most recently phonon dispersions and vibrational properties of monolayer, bilayer, and trilayer graphene have been calculated by density-functional theory.[53] Compared with the monolayer, splittings of optical phonon branches at the Γ and the K points were investigated; in addition there is one (two) additional low-frequency mode ($\approx 90\ \text{cm}^{-1}$) at Γ in bilayer (trilayer) graphene. Our calculations will confirm the results of Ref. 53 and investigate the transition of graphene layers to graphite as a function of the number N of layers. Electron diffraction experiments[54] have shown that multilayer graphene has the same stacking as graphite. The evolution of the electronic structure from a single graphene layer to bulk graphite has been studied by a tight-binding

theory approach.[40] Experimentally the change in the electronic bands at the K point in graphene layers is reflected in the change of the second-order double-resonance Raman spectrum.[54] In the present paper we restrict ourselves to the study of the phonon-dispersion laws in absence of electron-phonon coupling.

We start with the consideration of the case $N=2$: two graphene planes related by a screw diad axis (i.e., one α plane and one β plane) and separated by a distance $c/2$. The dynamical matrix of dimension 12×12 (i.e., $6N\times 6N$) is again written in terms of 6×6 submatrices $\mathcal{D}^{\alpha\alpha},\mathcal{H}^{\alpha\beta},\ldots$,

$$\mathcal{D}_2(\vec{q}_\perp)=\begin{bmatrix}\mathcal{D}^{\alpha\alpha}(\vec{q}_\perp) & \mathcal{H}^{\alpha\beta}(\vec{q}_\perp)\\ \mathcal{H}^{\beta\alpha}(\vec{q}_\perp) & \mathcal{D}^{\beta\beta}(\vec{q}_\perp)\end{bmatrix}. \tag{83}$$

Here, $\mathcal{D}^{\alpha\alpha},\mathcal{H}^{\alpha\beta},\ldots$ are given by

$$\mathcal{D}^{\alpha\alpha}(\vec{q}_\perp)=\begin{bmatrix}\mathcal{H}^{AA}+F^{AA}(\vec{q}_\perp) & F^{AB}(\vec{q}_\perp)\\ F^{BA}(\vec{q}_\perp) & \mathcal{H}^{BB}+F^{BB}(\vec{q}_\perp)\end{bmatrix}, \tag{84a}$$

$$\mathcal{D}^{\beta\beta}(\vec{q}_\perp)=\mathcal{D}^{\alpha\alpha}(\vec{q}_\perp)^*, \tag{84b}$$

$$\mathcal{H}^{\alpha\beta}(\vec{q}_\perp)=\begin{bmatrix}\mathcal{H}^{AA'}(\vec{q}_\perp) & \mathcal{H}^{AB'}(q_\perp)\\ \mathcal{H}^{BA'}(\vec{q}_\perp) & \mathcal{H}^{BB'}(\vec{q}_\perp)\end{bmatrix}, \tag{84c}$$

$$\mathcal{H}^{AA}=-[\mathcal{H}^{AA'}(\vec{q}_\perp=\vec{0})+\mathcal{H}^{AB'}(\vec{q}_\perp=\vec{0})], \tag{84d}$$

$$\mathcal{H}^{BB}=-[\mathcal{H}^{BA'}(\vec{q}_\perp=\vec{0})+\mathcal{H}^{BB'}(\vec{q}_\perp=\vec{0})]. \tag{84e}$$

The 3×3 matrices $F^{AA}(\vec{q}_\perp)$ and $F^{AB}(\vec{q}_\perp)$ refer to a single graphene plane, and are given by Eqs. (23a) and (23b), respectively. The 3×3 matrices $\mathcal{H}^{AA'}(\vec{q}_\perp),\mathcal{H}^{AB'}(\vec{q}_\perp),\ldots$ refer to interplanar couplings, they are quoted explicitly in Appendix C. Notice that these quantities depend on $\vec{q}_\perp$ since the system is extended in the directions [100] and [010]. The matrix $\mathcal{D}^{\alpha\alpha}(\vec{q}_\perp)$ is different from the matrix $D^{\alpha\alpha}(\vec{q}_\perp)$ [Eq. (25a)] in the graphite case since $\mathcal{H}^{AA'}(\vec{q}_\perp)$ and $\mathcal{H}^{AB'}(\vec{q}_\perp)$ differ from $H^{AA'}(\vec{q})$ and $H^{AB'}(\vec{q})$, respectively (see Appendices B and C). The phonon spectrum of the two layer slab is obtained by solving the secular problem for the dynamical matrix $\mathcal{D}_2(q_\perp)$.

The formulation is readily extended to the problem with $N\geq 3$ layers by observing that the upper and lower boundary layers interact only with one neighboring layer while each layer in the bulk interacts with two neighboring layers at distance $Z=+c/2$ and $Z=-c/2$. Here one obtains for three layers a 18×18 dynamical matrix with the 6×6 submatrices structure

$$\mathcal{D}_3(\vec{q}_\perp)=\begin{bmatrix}\mathcal{D}^{\alpha\alpha}(\vec{q}_\perp) & \mathcal{H}^{\alpha\beta}(\vec{q}_\perp) & 0\\ \mathcal{H}^{\beta\alpha}(\vec{q}_\perp) & \Delta(\vec{q}_\perp)^* & \mathcal{H}^{\beta\alpha}(\vec{q}_\perp)\\ 0 & \mathcal{H}^{\alpha\beta}(\vec{q}_\perp) & \mathcal{D}^{\alpha\alpha}(\vec{q}_\perp)\end{bmatrix}, \tag{85}$$

with

$$\Delta(\vec{q}_\perp)=\begin{bmatrix}2\mathcal{H}^{AA}+F^{AA}(\vec{q}_\perp) & F^{AB}(\vec{q}_\perp)\\ F^{BA}(\vec{q}_\perp) & 2\mathcal{H}^{BB}+F^{BB}(\vec{q}_\perp)\end{bmatrix}. \tag{86}$$

The dynamical matrix of the N layer problem reads

$$\mathcal{D}_N(\vec{q}_\perp)=\begin{bmatrix}\mathcal{D}^{\alpha\alpha}(\vec{q}_\perp) & \mathcal{H}^{\alpha\beta}(\vec{q}_\perp) & 0 & 0 & \ldots & 0 & 0\\ \mathcal{H}^{\beta\alpha}(\vec{q}_\perp) & \Delta(\vec{q}_\perp)^* & \mathcal{H}^{\beta\alpha}(\vec{q}_\perp) & 0 & \ldots & 0 & 0\\ 0 & \mathcal{H}^{\alpha\beta}(\vec{q}_\perp) & \Delta(\vec{q}_\perp) & \mathcal{H}^{\alpha\beta}(\vec{q}_\perp) & \ldots & 0 & 0\\ 0 & 0 & \mathcal{H}^{\beta\alpha}(\vec{q}_\perp) & \Delta(\vec{q}_\perp)^* & \ldots & 0 & 0\\ \vdots & \vdots & \vdots & \vdots & \ddots & \vdots & \vdots\\ 0 & 0 & 0 & 0 & \ldots & \Delta(\vec{q}_\perp)^{(*)} & \mathcal{H}^{\kappa'\kappa}(\vec{q}_\perp)\\ 0 & 0 & 0 & 0 & \ldots & \mathcal{H}^{\kappa\kappa'}(\vec{q}_\perp) & \mathcal{D}^{\kappa\kappa}(\vec{q}_\perp)\end{bmatrix}, \tag{87}$$

where $\kappa=\alpha$ and $\kappa'=\beta$ for N even, and $\kappa=\beta$ and $\kappa'=\alpha$ for N uneven.

Phonon-dispersion relations for slabs of N layers, obtained by solving the secular equation with the dynamical matrix $\mathcal{D}_N(\vec{q}_\perp)$, are shown in Fig. 5. Again, as is the case for graphite, the spectra at frequencies above 200 cm^{-1} exhibit the six graphene bands. The splitting of the lowest acoustic A_{2u} mode band in the neighborhood of the Γ point leads to the lowest acoustic mode (A_{2u}) and to $N-1$ optical modes of B_{2g_1} symmetry, which extends the results on bilayer and trilayer graphene.[53] As a function of increasing N, the highest of these optical modes that we denote by $\omega^{(N)}_{B_{2g_1}}$ tends to a limit value at the zone center, which corresponds to the value of the ≈ 127 cm^{-1} B_{2g_1} mode of graphite at the Γ point. As is shown in Fig. 6, where we have plotted $\omega^{(N)}_{B_{2g_1}}$ as a function of N, the limit value $\omega_{B_{2g_1}}$ is practically reached near $N=15$. The situation is reminiscent of the evolution of the electronic structure of graphene multilayers near the K point. There for $N=11$ and more layers, the difference in band overlap with graphite is smaller than 10%.[40]

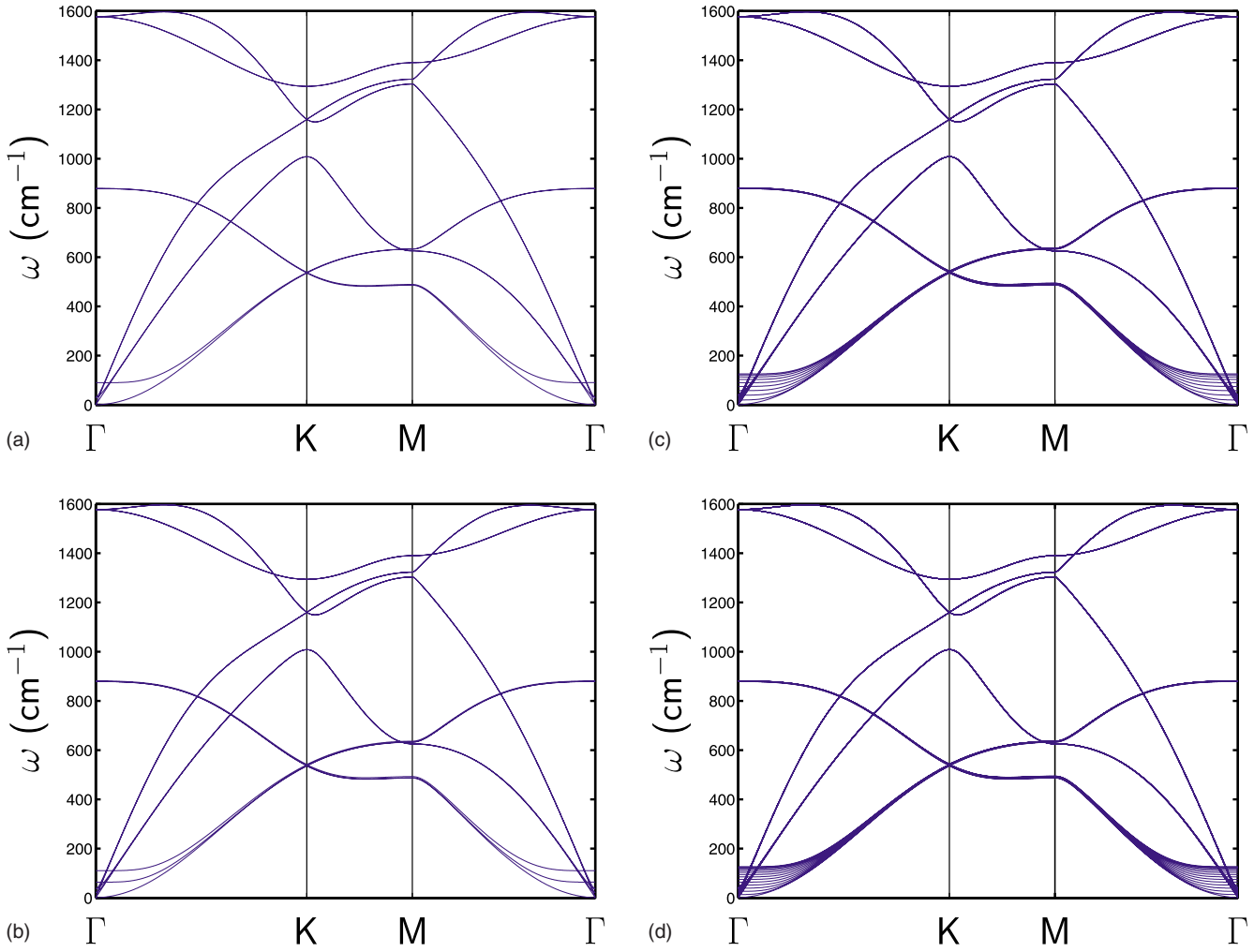

FIG. 5. (Color online) Phonon spectra for graphene multilayers.

VII. CONCLUDING REMARKS

We have presented a unified theoretical treatment of the lattice dynamics of graphene, graphite, and graphene multilayers within a harmonic phonon approach.

In constructing the dynamical matrix of graphene, we start from the fifth-neighbor force constants derived from empirical phonon-dispersion relations.[30] Using Born's long-wave method for the evaluation of elastic constants, we have calculated the tension coefficients $\gamma_{11}=40.55\times10^4$ dyn/cm and $\gamma_{12}=9.24\times10^4$ dyn/cm, as well as the sound velocities $c_l=23.08$ km/s and $c_t=14.34$ km/s, the Young's modulus $Y_{2D}=38.46\times10^4$ dyn/cm, and the Poisson ratio $\sigma_{2D}=0.228$ of graphene. We have found that the inner displacement terms due to relative shifts between A and B sublattices are quantitatively important in determining the elastomechanical properties of graphene. We have calculated the bending rigidity of graphene and obtain a value of $\tilde{\kappa}_b=1.12$ eV.

We have extended the force-constant model to graphite by taking into account *ad hoc* force-constant values for nearest-neighbor interlayer A-A atom interactions and a Lennard-Jones potential for A-B atom interactions. We have calculated the phonon-dispersion relations (Fig. 4), the optical phonons at the Brillouin-zone center (Table I), and the elastic constants of graphite. Here too (Sec. V) we find that the inner displacement terms due to sublattice shifts within single graphite planes are quantitatively important; on the other hand, shifts of sublattices belonging to different planes are negligible. The agreement between our theoretical values of the elastic constants and sound velocities with recent experimental single-crystal IXS results[28] is remarkable. We have established (end of Sec. V) approximate relations between the elastic constants c_{11} and c_{66} of graphite, and the tension coefficients γ_{11} and γ_{66}, respectively, of graphene. These relations explain why the longitudinal and transverse sound velocities c_l and c_t of graphene have values close to the corresponding quantities of graphite. Thereby a theoretical foundation is provided for the experimental strategy that full in-plane IXS phonon dispersions on single crystals of graphite[30] are representative for graphene and relevant for the understanding of the elastic properties of carbon nanotubes.[20]

Finally we have solved the secular equation and calculated phonon-dispersion relations for the N graphene layers system. The frequency $\omega^{(N)}_{B_{2g_1}}$ of the out-of-plane rigid layer optical displacements increases with the number of layers N.

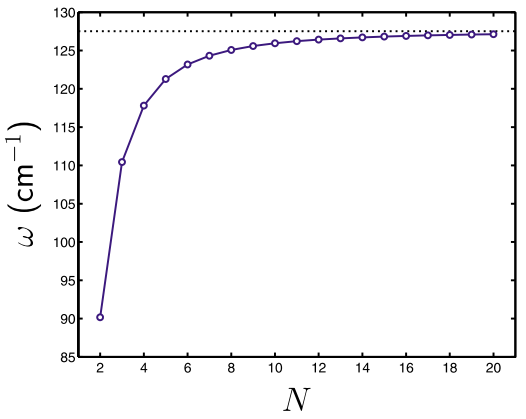

FIG. 6. (Color online) Evolution of the optical eigenmode $\omega_{B_{2g_1}}^{(N)}$ with increasing number of graphene layers.

Starting from $\omega_{B_{2g_1}}^{(2)} \approx 90$ cm^{-1}, we find that at $N=10$ the graphite value $\omega_{B_{2g_1}} = 127$ cm^{-1} is attained within a few percent. However we recall that this mode is optically silent;[7] in bulk it can be measured by INS and IXS. The evolution of this mode in layered structures might be accessible by high-resolution helium atom scattering.[55]

ACKNOWLEDGMENTS

The authors acknowledge useful discussion with B. Partoens. F.M. Peeters informed us about some important references. This work has been supported by the Flemish Science Foundation (Fonds voor Wetenschappelijk Onderzoek-Vlaanderen) and the Bijzonder Onderzoeksfonds, Universiteit Antwerpen.

APPENDIX A

We calculate the elements of the 6×6 dynamical matrix $F(\vec{q}_\perp)$ of graphene by using empirical interatomic force parameters up to fifth-nearest neighbors as introduced in Ref. 30. These force parameters mimic the covalent bond forces within the graphene plane. The parameters $f_r^{(n)}$, $f_i^{(n)}$, and $f_o^{(n)}$ with $n=1,2,\ldots,5$ refer to the radial (bond-stretching), in-plane, and out-of-plane tangential (bond-bending) directions of the nth C-C neighbors, respectively. For the sake of completeness, we quote again the values in Table V. Starting from a bond between atoms at $(\vec{n}_\perp \kappa)$ and $(\vec{n}'_\perp \kappa')$ where the force constants are the diagonal elements of a 3×3 second-rank tensor, the corresponding Cartesian components

TABLE V. Force-constant parameters of Ref. 30 in eV/Å^2.

n	$f_r^{(n)}$	$f_i^{(n)}$	$f_o^{(n)}$
1	25.880	8.420	6.183
2	4.037	−3.044	−0.492
3	−3.016	3.948	0.516
4	0.564	0.129	−0.521
5	1.035	0.166	0.110

$f_{ij}^{(n)}(\vec{n}_\perp \kappa;\vec{n}'_\perp \kappa')$ are obtained by appropriate rotations about the Z axis perpendicular to the graphene plane. The elements of the dynamical matrix then follow from Eqs. (23a)–(23d). Here we quote the terms $F_{ij}^{(n)\kappa\kappa'}(\vec{q})$. The elements of the dynamical matrix are then obtained as

$$F_{ij}^{\kappa\kappa'}(\vec{q}_\perp) = \sum_{n=1}^{5} F_{ij}^{(n)\kappa\kappa'}(\vec{q}). \tag{A1}$$

The first neighbors of a given A atom at (0,0) are three B atoms at $(\frac{1}{\sqrt{3}},0)a$, $(-\frac{1}{2\sqrt{3}},\pm\frac{1}{2})a$. We obtain

$$F_{xx}^{(1)AA}(\vec{q}_\perp) = F_{yy}^{(1)AA} = \frac{3}{2M}[f_r^{(1)} + f_i^{(1)}], \tag{A2a}$$

$$F_{zz}^{(1)AA}(\vec{q}_\perp) = \frac{3}{M} f_o^{(1)}. \tag{A2b}$$

All other elements of $F^{(1)AA}(\vec{q}_\perp)$ are zero. Furthermore

$$F_{xx}^{(1)AB}(\vec{q}_\perp) = -\frac{1}{M}\left\{ f_r^{(1)} e^{iq_x a/\sqrt{3}} + \frac{1}{2}[f_r^{(1)} + 3f_i^{(1)}]\cos\left(\frac{q_y a}{2}\right) e^{-iq_x a/2\sqrt{3}} \right\}, \tag{A3}$$

where $F_{yy}^{(1)AB}(\vec{q}_\perp)$ is obtained by interchanging f_r with f_i, $F_{zz}^{(1)AB}(\vec{q}_\perp)$ is obtained from $F_{xx}^{(1)AB}(\vec{q}_\perp)$ by replacing both $f_r^{(1)}$ and $f_i^{(1)}$ by $f_o^{(1)}$,

$$F_{xy}^{(1)AB}(\vec{q}_\perp) = \frac{i\sqrt{3}}{2M}[f_r^{(1)} - f_i^{(1)}]\sin\left(\frac{q_y a}{2}\right) e^{-iq_x a/2\sqrt{3}}. \tag{A4}$$

All other elements of $F^{(1)AB}(\vec{q}_\perp)$ are zero.

The contributions due to second-neighbor A atoms located at $(0,\pm 1)a$, $\frac{1}{2}(\pm\sqrt{3},1)a$, and $\frac{1}{2}(\pm\sqrt{3},-1)a$ are

$$F_{xx}^{(2)AA}(\vec{q}_\perp) = \frac{1}{M}\left\{ [f_i^{(2)} + 3f_r^{(2)}]\left[\sin^2(\sqrt{3}q_x + q_y)\frac{a}{4} + \sin^2(-\sqrt{3}q_x + q_y)\frac{a}{4}\right] + 4f_i^{(2)}\sin^2\left(\frac{q_y a}{2}\right)\right\}, \tag{A5}$$

where $F_{yy}^{(2)AA}(\vec{q}_\perp)$ is obtained by interchanging f_r and f_i, $F_{zz}^{(2)AA}(\vec{q}_\perp)$ is obtained by replacing both $f_i^{(2)}$ and $f_r^{(2)}$ by $f_o^{(2)}$,

$$F_{xy}^{(2)AA}(\vec{q}_\perp) = -\frac{\sqrt{3}}{M}[f_i^{(2)} - f_r^{(2)}]\left[\sin^2(\sqrt{3}q_x + q_y)\frac{a}{4} - \sin^2(-\sqrt{3}q_x + q_y)\frac{a}{4}\right]. \tag{A6}$$

All other terms of $F^{(2)AA}(\vec{q}_\perp)$ and all terms of $F^{(2)AB}(\vec{q}_\perp)$ are zero.

The third-neighbor B atoms at $(-\frac{2}{\sqrt{3}},0)a$ and $(\frac{1}{\sqrt{3}},\pm 1)a$ account for $F^{(3)AA}(\vec{q}_\perp)$ and $F^{(3)AB}(\vec{q}_\perp)$. The elements are obtained from the first-neighbor elements by replacing $f_r^{(1)}$, $f_i^{(1)}$, and $f_o^{(1)}$ by $f_r^{(3)}$, $f_i^{(3)}$, and $f_o^{(3)}$, respectively, and by replacing a in the phase factors by $-2a$.

The fourth-neighbor B atoms at $(\frac{5}{2\sqrt{3}},\pm\frac{1}{2})a$, $(-\frac{1}{2\sqrt{3}},\pm\frac{3}{2})a$, and $(-\frac{2}{\sqrt{3}},\pm 1)a$ lead to the following results. The elements

TABLE VI. Interplanar force constants $h_{ij}(0;\nu)$ with units in dyn/cm. Values in brackets are chosen *ad hoc*—see Sec. III B.

ν	1_+	$1'_+$	$2'_+$	$1''_+$	$2''_+$
$h_{11}(0;\nu)$	−114.47(400.00)	63.17	2.73	8.95	6.31
$h_{22}(0;\nu)$	−114.47(400.00)	−17.41	43.02	7.19	9.83
$h_{33}(0;\nu)$	2040.41(1800.00)	430.87	430.87	12.84	12.84
$h_{12}(0;\nu)$	0	0	−34.89	1.52	0
$h_{13}(0;\nu)$	0	−190.05	95.03	4.15	0
$h_{23}(0;\nu)$	0	0	−164.59	2.40	4.79

of $F^{(4)AA}$ are obtained from those of $F^{(1)AA}$ by replacing $f_r^{(1)}$, $f_i^{(1)}$, and $f_o^{(1)}$ by $2f_r^{(4)}$, $2f_i^{(4)}$, and $2f_o^{(4)}$, respectively. Furthermore

$$F_{xx}^{(4)AB}(\vec{q}_\perp) = -\frac{2}{M}\Bigg\{[f_r^{(4)}\cos^2\theta_1 + f_i^{(4)}\sin^2\theta_1]e^{iq_x 5a/2\sqrt{3}}\cos\left(\frac{q_y a}{2}\right) + [f_r^{(4)}\cos^2\theta_2 + f_i^{(4)}\sin^2\theta_2]e^{-iq_x a/2\sqrt{3}}\cos\left(\frac{3q_y a}{2}\right) + [f_r^{(4)}\cos^2\theta_3 + f_i^{(4)}\sin^2\theta_3]e^{-iq_x 2a/\sqrt{3}}\cos(q_y a)\Bigg\}, \tag{A7}$$

where $\theta_1 = \arctan(\frac{\sqrt{3}}{5})$, $\theta_2 = \frac{2\pi}{3} - \theta_1$, and $\theta_3 = \frac{2\pi}{3} + \theta_1$. The element $F_{yy}^{(4)AB}(\vec{q}_\perp)$ is obtained by interchange of $f_r^{(4)}$ and $f_i^{(4)}$ in $F_{xx}^{(4)AB}(\vec{q}_\perp)$ while $F_{zz}^{(4)AB}(\vec{q}_\perp)$ is obtained by replacing $f_r^{(4)}$ and $f_i^{(4)}$ by $f_o^{(4)}$. Furthermore

$$F_{xy}^{(4)AB}(\vec{q}_\perp) = -\frac{i}{M}[f_r^{(4)} - f_i^{(4)}]\Bigg[\sin(2\theta_1)e^{iq_x 5a/2\sqrt{3}}\sin\left(\frac{q_y a}{2}\right) + \sin(2\theta_2)e^{-iq_x a/2\sqrt{3}}\sin\left(\frac{3q_y a}{2}\right) + \sin(2\theta_3)e^{-iq_x 2a/\sqrt{3}}\sin(q_y a)\Bigg]. \tag{A8}$$

The elements of $F^{(5)AA}(\vec{q}_\perp)$ due to the fifth-neighbor atoms A at $\frac{1}{2}(\sqrt{3},\pm 3)a$, $\frac{1}{2}(-\sqrt{3},\pm 3)a$, and $(\pm\sqrt{3},0)a$ are obtained from the second-neighbor elements of $F^{(2)AA}(\vec{q}_\perp)$ by replacing $f_i^{(2)}$ by $f_r^{(5)}$, $f_r^{(2)}$ by $f_i^{(5)}$, and $f_o^{(2)}$ by $f_o^{(5)}$, respectively. In addition one has to interchange q_x with q_y and to replace a by $\sqrt{3}a$. The coefficients $F_{ij}^{\kappa\kappa'(0)}$, $F_{ij,k}^{\kappa\kappa'(1)}$, and $F_{ij,kl}^{\kappa\kappa'(2)}$ in Eq. (32) are obtained from expansion of the elements $F_{ij}^{\kappa\kappa'}(\vec{q}_\perp)$ [Eq. (A1)] in powers of the wave-vector components (q_x, q_y).

APPENDIX B

We calculate the interplane force constants $h_{ij}(\vec{n}\kappa;\vec{n}'\kappa')$ by retaining only interactions between next neighbor graphene planes. We start from an empirical Lennard-Jones potential [Eq. (30)]. The force constants h_{ij} are defined by

$$h_{ij}(\vec{n}\kappa;\vec{n}'\kappa') = \frac{\partial^2 V(r)}{\partial x_i(\vec{n}\kappa;\vec{n}'\kappa')\,\partial x_j(\vec{n}\kappa;\vec{n}'\kappa')}, \tag{B1}$$

taken at $\vec{u}(\vec{n}\kappa;\vec{n}'\kappa') = \vec{0}$. Each A atom at equilibrium $(0,0,0) = \vec{x}(0)$, taken as origin, interacts with two A' atoms at $(0,0,\pm\frac{c}{2})$ as nearest neighbors with six B' atoms at $(-\frac{a}{\sqrt{3}},0,\pm\frac{c}{2})$, $(\frac{a}{2\sqrt{3}},\frac{a}{2},\pm\frac{c}{2})$, and $(\frac{a}{2\sqrt{3}},-\frac{a}{2},\pm\frac{c}{2})$ as second neighbors, and with twelve A' atoms at $(\pm\frac{\sqrt{3}}{2}a,\pm\frac{a}{2},\pm\frac{c}{2})$ and $(0,\pm a,\pm\frac{c}{2})$ as third neighbors (lattice-parameter values $a = 2.46$ Å and $c = 6.70$ Å). We label the first-neighbor A' atoms by $\nu = 1_+$ and 1_- corresponding to the planes $z = +c/2$ and $z = -c/2$, respectively; similarly we label the second-neighbor B' atoms by $\nu = 1'_+, 2'_+, 3'_+$ and $1_-, 2_-, 3_-$, respectively, and the third-neighbor A' atoms by $\nu = 1''_+, \ldots, 6''_+$ and $1_-, \ldots, 6_-$, respectively. The force constants read

$$h_{ij}(0;\nu) = \frac{x_i(0;\nu)x_j(0;\nu)}{r_\nu^2}\left[V''(r_\nu) - \frac{V'(r_\nu)}{r_\nu}\right] + \delta_{ij}\frac{V'(r_\nu)}{r_\nu}, \tag{B2}$$

where $r_\nu = |\vec{x}(0;\nu)| \equiv |\vec{x}(\nu) - \vec{x}(0)|$ is the equilibrium distance. Numerical values are quoted in Table VI. From Eq. (27) we obtain, by using the symmetry of the crystal structure,

$$H_{ii}^{AA'}(\vec{q}) = -\frac{2}{M}\Bigg\{h_{ii}(0;1_+) + 2\left[\begin{matrix}2h_{ii}(0;1''_+)\cos\left(\frac{q_x\sqrt{3}a}{2}\right)\cos\left(\frac{q_y a}{2}\right) \\ + h_{ii}(0;2''_+)\cos(q_y a)\end{matrix}\right]\Bigg\}\cos\left(\frac{q_z c}{2}\right), \tag{B3a}$$

$$H_{12}^{AA'}(\vec{q}) = \frac{8}{M}h_{12}(0;1''_+)\sin\left(\frac{q_x\sqrt{3}a}{2}\right)\sin\left(\frac{q_y a}{2}\right)\cos\left(\frac{q_z c}{2}\right), \tag{B3b}$$

$$H_{13}^{AA'}(\vec{q}) = \frac{8}{M}h_{13}(0;1''_+)\sin(q_x\sqrt{3}a/2)\cos\left(\frac{q_y a}{2}\right)\sin\left(\frac{q_z c}{2}\right), \tag{B3c}$$

$$H_{23}^{AA'}(\vec{q}) = \frac{4}{M}\Bigg[2h_{23}(0;1''_+)\sin\left(\frac{q_y a}{2}\right)\cos\left(\frac{q_x\sqrt{3}a}{2}\right) + h_{23}(0;2''_+)\sin(q_y a)\Bigg]\sin\left(\frac{q_z c}{2}\right). \tag{B3d}$$

The labels ν refer to the positions $1'_+=(0,0,c/2)$, $1''_+=(a\sqrt{3}/2,a/2,c/2)$, and $2''_+=(0,a,c/2)$. Furthermore,

$$H_{ii}^{AB'}(\vec{q}) = -\frac{2}{M}\left[h_{ii}(0;1'_+)e^{-iq_xa/\sqrt{3}} + 2h_{ii}(0;2'_+)\cos\left(q_y\frac{a}{2}\right)e^{iq_xa/2\sqrt{3}}\right]\cos\left(\frac{q_zc}{2}\right), \tag{B4a}$$

$$H_{12}^{AB'}(\vec{q}) = -\frac{4i}{M}h_{12}(0;2'_+)\sin\left(\frac{q_ya}{2}\right)e^{iq_xa/2\sqrt{3}}\cos\left(\frac{q_zc}{2}\right), \tag{B4b}$$

$$H_{13}^{AB'}(\vec{q}) = -\frac{2i}{M}\left[h_{13}(0;1'_+)e^{-iq_xa/\sqrt{3}} + 2h_{13}(0;2'_+)e^{iq_xa/2\sqrt{3}}\cos\left(\frac{q_ya}{2}\right)\right]\sin\left(\frac{q_zc}{2}\right), \tag{B4c}$$

$$H_{23}^{AB'}(\vec{q}) = \frac{4}{M}h_{23}(0;2'_+)e^{iq_xa/2\sqrt{3}}\sin\left(\frac{q_ya}{2}\right)\sin\left(\frac{q_zc}{2}\right). \tag{B4d}$$

Here the labels refer to the positions $1'_+=(-\frac{a}{\sqrt{3}},0,\frac{c}{2})$ and $2'_+=(\frac{a}{2\sqrt{3}},\frac{a}{2},\frac{c}{2})$.

In a similar way we calculate the interactions of a $-\frac{1}{2}$ atom at (0,0,0) taken as origin with six B' atoms at $(\frac{a}{\sqrt{3}},0,\pm\frac{c}{2})$, $(-\frac{a}{2\sqrt{3}},\frac{a}{2},\pm\frac{c}{2})$, and $(-\frac{a}{2\sqrt{3}},-\frac{a}{2},\pm\frac{c}{2})$. Symmetry of the crystal entails that we can use the same force constants as defined for the A-B' interactions. We obtain

$$H^{BB'}(\vec{q}) = H^{AB'}(\vec{q})^*. \tag{B5}$$

The interaction of a B atom at (0,0,0) with six A' atoms at $(-\frac{a}{\sqrt{3}},0,\pm\frac{c}{2})$, $(\frac{a}{2\sqrt{3}},\pm\frac{a}{2},\pm\frac{c}{2})$ gives

$$H^{BA'}(\vec{q}) = H^{AB'}(\vec{q}). \tag{B6}$$

APPENDIX C

Here we give the interplanar coupling matrix elements $\mathcal{H}^{\kappa\kappa'}(\vec{q}_\perp)$ for the graphite slab problem. We have, for the interactions of an A atom in an α plane with one nearest-neighbor A' atom and six third-neighbor A' atoms in the neighboring β plane, the elements

$$\mathcal{H}_{ii}^{AA'}(\vec{q}_\perp) = -\frac{1}{M}\left\{h_{ii}(0;1_+) + 2\left[2h_{ii}(0;1''_+)\cos\left(\frac{q_x\sqrt{3}a}{2}\right)\cos\left(\frac{q_ya}{2}\right) + h_{ii}(0;2''_+)\cos(q_ya)\right]\right\}, \tag{C1a}$$

$$\mathcal{H}_{12}^{AA'}(\vec{q}_\perp) = \frac{4}{M}h_{12}(0;1''_+)\sin\left(\frac{q_x\sqrt{3}a}{2}\right)\sin\left(\frac{q_ya}{2}\right), \tag{C1b}$$

$$\mathcal{H}_{13}^{AA'}(\vec{q}_\perp) = -\frac{4i}{M}h_{13}(0;1''_+)\sin(q_x\sqrt{3}a/2)\cos\left(\frac{q_ya}{2}\right), \tag{C1c}$$

and

$$\mathcal{H}_{23}^{AA'}(\vec{q}_\perp) = -\frac{2i}{M}\left\{2h_{23}(0;1''_+)\sin\left(\frac{q_ya}{2}\right)\cos\left(\frac{q_x\sqrt{3}a}{2}\right) + h_{23}(0;2''_+)\sin(q_ya)\right\}. \tag{C1d}$$

The force constants are those quoted in Table VI in Appendix B. The interactions of an A atom with three second-neighbor B' atoms are given by

$$\mathcal{H}_{ii}^{AB'}(\vec{q}_\perp) = -\frac{1}{M}\left[h_{ii}(0;1'_+)e^{-\frac{iq_xa}{\sqrt{3}}} + 2h_{ii}(0;2'_+)\cos\left(q_y\frac{a}{2}\right)e^{\frac{iq_xa}{2\sqrt{3}}}\right], \tag{C2a}$$

$$\mathcal{H}_{12}^{AB'}(\vec{q}_\perp) = -\frac{2i}{M}h_{12}(0;2'_+)\sin\left(\frac{q_ya}{2}\right)e^{\frac{iq_xa}{2\sqrt{3}}}, \tag{C2b}$$

$$\mathcal{H}_{13}^{AB'}(\vec{q}_\perp) = -\frac{1}{M}\left[h_{13}(0;1'_+)e^{-i\frac{q_xa}{\sqrt{3}}} + 2h_{13}(0;2'_+)e^{i\frac{q_xa}{2\sqrt{3}}}\cos\left(\frac{q_ya}{2}\right)\right], \tag{C2c}$$

and

$$\mathcal{H}_{23}^{AB'}(\vec{q}_\perp) = -\frac{2i}{M}h_{23}(0;2'_+)e^{i\frac{q_xa}{2\sqrt{3}}}\sin\left(\frac{q_ya}{2}\right). \tag{C2d}$$

The interactions of a B atom with three nearest-neighbor B' atoms are

$$\mathcal{H}_{ii}^{BB'}(\vec{q}_\perp) = \mathcal{H}_{ii}^{AB'}(\vec{q}_\perp)^*, \tag{C3a}$$

$$\mathcal{H}_{12}^{BB'}(\vec{q}_\perp) = \mathcal{H}_{12}^{AB'}(\vec{q}_\perp)^*, \tag{C3b}$$

$$\mathcal{H}_{13}^{BB'}(\vec{q}_\perp) = -\mathcal{H}_{12}^{AB'}(\vec{q}_\perp)^*, \tag{C3c}$$

and

$$\mathcal{H}_{23}^{BB'}(\vec{q}_\perp) = -\mathcal{H}_{23}^{AB'}(\vec{q}_\perp)^*. \tag{C3d}$$

[1] M. S. Dresselhaus, G. Dresselhaus, and P. C. Eklund, *Science of Fullerenes and Carbon Nanotubes* (Academic, San Diego, 1996).
[2] R. Saito, G. Dresselhaus, and M. S. Dresselhaus, *Physical Properties of Carbon Nanotubes* (Imperial College, London, 1998).
[3] G. Dolling and B. N. Brockhouse, Phys. Rev. **128**, 1120 (1962).
[4] R. Nicklow, N. Wakabayashi, and H. G. Smith, Phys. Rev. B **5**, 4951 (1972).
[5] O. L. Blakslee, D. G. Proctor, E. J. Seldin, G. B. Spence, and T. Weng, J. Appl. Phys. **41**, 3373 (1970); E. J. Seldin and C. W. Nezbeda, *ibid.* **41**, 3389 (1970).
[6] A. F. Tuinstra and J. L. Koenig, J. Chem. Phys. **53**, 1126 (1970).
[7] R. J. Nemanich, G. Lucovsky, and S. A. Solin, Solid State Commun. **23**, 117 (1977).
[8] K. K. Mani and R. Ramani, Phys. Status Solidi B **61**, 659 (1974).
[9] A. P. P. Nicholson and D. J. Bacon, J. Phys. C **10**, 2295 (1977).
[10] M. Maeda, Y. Kuramoto, and C. Horie, J. Phys. Soc. Jpn. **47**, 337 (1979).
[11] R. Al-Jishi and G. Dresselhaus, Phys. Rev. B **26**, 4514 (1982).
[12] B. T. Kelly, *Physics of Graphite* (Applied Science, London, 1981).
[13] C. Oshima, T. Aizawa, R. Souda, Y. Ishizawa, and Y. Sumiyoshi, Solid State Commun. **65**, 1601 (1988).
[14] P. Pavone, R. Bauer, K. Karch, O. Schütt, S. Vent, W. Windl, D. Strauch, S. Baroni, and S. de Gironcoli, Physica B (Amsterdam) **219-220**, 439 (1996).
[15] J. C. Boettger, Phys. Rev. B **55**, 11202 (1997).
[16] P. R. Wallace, Phys. Rev. **71**, 622 (1947); **72**, 258 (1947).
[17] J. W. McClure, Phys. Rev. **104**, 666 (1956).
[18] J. C. Slonczewski and P. R. Weiss, Phys. Rev. **109**, 272 (1958).
[19] A. V. Nikolaev and B. Verberck, in *Carbon-Based Magnetism*, edited by T. Makarova and F. Palacio (Elsevier, Amsterdam, 2006), p. 245.
[20] S. Reich, C. Thomsen, and J. Maultzsch, *Carbon Nanotubes* (Wiley, Weinheim, 2003); *Understanding Carbon Nanotubes*, edited by A. Loiseau, P. Launois, P. Petit, S. Roche, and J.-P. Salvetat (Springer-Verlag, Berlin, 2006).
[21] J. Jiang, R. Saito, A. Grüneis, S. G. Chou, Ge. G. Samsonidze, A. Jorio, G. Dresselhaus, and M. S. Dresselhaus, Phys. Rev. B **71**, 205420 (2005); J. Jiang, R. Saito, Ge. G. Samsonidze, S. G. Chou, A. Jorio, G. Dresselhaus, and M. S. Dresselhaus, *ibid.* **72**, 235408 (2005).
[22] N. D. Mermin and H. Wagner, Phys. Rev. Lett. **17**, 1133 (1966); N. D. Mermin, Phys. Rev. **176**, 250 (1968).
[23] K. S. Novoselov, A. K. Geim, S. V. Morosov, D. Jiang, Y. Zhang, S. V. Dubonos, I. V. Grigorieva, and A. A. Frisov, Science **306**, 666 (2004).
[24] K. S. Novoselov, D. Jiang, F. Schedin, T. J. Booth, V. V. Khotkerrick, S. V. Morosov, and A. K. Geim, Proc. Natl. Acad. Sci. U.S.A. **102**, 10451 (2005).
[25] For a review, see A. K. Geim and K. S. Novoselov, Nat. Mater. **6**, 183 (2007).
[26] J. C. Meyer, A. K. Geim, M. I. Katsnelson, K. S. Novoselov, D. Obergfell, S. Roth, C. Girit, and A. Zettl, Nature (London) **446**, 60 (2007).
[27] A. Fasolino, J. H. Los, and M. I. Katsnelson, Nat. Mater. **6**, 858 (2007).
[28] A. Bosak, M. Krisch, M. Mohr, J. Maultzsch, and C. Thomsen, Phys. Rev. B **75**, 153408 (2007).
[29] J. Maultzsch, S. Reich, C. Thomsen, H. Requardt, and P. Ordejón, Phys. Rev. Lett. **92**, 075501 (2004).
[30] M. Mohr, J. Maultzsch, E. Dobardzic, S. Reich, I. Milosevic, M. Damnjanovic, A. Bosak, M. Krisch, and C. Thomsen, Phys. Rev. B **76**, 035439 (2007).
[31] See, e.g., A. A. Maradudin, E. W. Montroll, G. H. Weiss, and I. P. Ipatova, in *Theory of Lattice Dynamics in the Harmonic Approximation*, Solid State Physics Suppl. 3, edited by H. Ehrenreich, F. Seitz, and D. Turnbull (Academic, New York, 1971).
[32] M. Born and K. Huang, *Dynamical Theory of Crystal Lattices* (Oxford University Press, New York, 1954).
[33] W. Götze and K. H. Michel, Z. Phys. **217**, 170 (1968).
[34] L. A. Girifalco and R. A. Lad, J. Chem. Phys. **25**, 693 (1956).
[35] L. A. Girifalco, M. Hodak, and R. S. Lee, Phys. Rev. B **62**, 13104 (2000).
[36] H. Yanagisawa, T. Tanaka, Y. Ishida, M. Matsue, E. Rokuta, S. Otani, and C. Oshima, Surf. Interface Anal. **37**, 133 (2005).
[37] O. Dubay and G. Kresse, Phys. Rev. B **67**, 035401 (2003).
[38] R. J. Nemanich, G. Lucovsky, and S. A. Solin, in Proceedings of the International Conference on Lattice Dynamics, edited by M. Balkanski (Flammarion, Paris, 1975), p. 619.
[39] L. G. Johnson and G. Dresselhaus, Phys. Rev. B **7**, 2275 (1973).
[40] B. Partoens and F. M. Peeters, Phys. Rev. B **74**, 075404 (2006); **75**, 193402 (2007).
[41] S. Piscanec, M. Lazzeri, F. Mauri, A. C. Ferrari, and J. Robertson, Phys. Rev. Lett. **93**, 185503 (2004).
[42] L. D. Landau and E. M. Lifshitz, *Elastizitätstheorie* (Akademie-Verlag, Berlin, 1987).
[43] F. I. Fedorov, *Theory of Elastic Waves in Crystals* (Plenum, New York, 1968).
[44] P. M. Chaikin and T. C. Lubensky, *Principles of Condensed Matter Physics* (Cambridge University Press, Cambridge, England, 1995).
[45] D. R. Nelson and L. Peliti, J. Phys. (Paris) **48**, 1085 (1987).
[46] H. J. F. Jansen and A. J. Freeman, Phys. Rev. B **35**, 8207 (1987).
[47] M. Grimsditch, J. Phys. C **16**, L143 (1983).
[48] M. Hanfland, H. Beister, and K. Syassen, Phys. Rev. B **39**, 12598 (1989).
[49] N. Mounet and N. Marzari, Phys. Rev. B **71**, 205214 (2005).
[50] C. A. Klein and M. G. Holland, Phys. Rev. **136**, A575 (1964).
[51] K. Komatsu, J. Phys. Soc. Jpn. **10**, 346 (1955); Phys. Chem. Solids **6**, 380 (1958).
[52] E. de Rouffignac, G. P. Alldredge, and F. W. de Wette, Phys. Rev. B **23**, 4208 (1981).
[53] J.-A. Yan, W. Y. Ruan, and M. Y. Chou, Phys. Rev. B **77**, 125401 (2008).
[54] A. C. Ferrari, J. C. Meyer, V. Scardaci, C. Casiraghi, M. Lazzeri, F. Mauri, S. Piscanec, D. Jiang, K. S. Novoselov, S. Roth, and A. K. Geim, Phys. Rev. Lett. **97**, 187401 (2006).
[55] G. Benedek, G. Brusdeylins, C. Heimlich, J. P. Toennies, and U. Valbusa, Surf. Sci. **178**, 545 (1986).